Atmos. Chem. Phys. Discuss., https://doi.org/10.5194/acp-2018-71
Manuscript under review for journal Atmos. Chem. Phys.
Discussion started: 26 January 2018

Atmospheric Chemistry and Physics Discussions

Evaluating High-Resolution Forecasts of Atmospheric CO and CO_2 from a Global Prediction System during KORUS-AQ Field Campaign

Wenfu Tang[1], Avelino F. Arellano[1], Joshua P. DiGangi[2], Yonghoon Choi[2,3], Glenn S. Diskin[2], Anna Agustí-Panareda[4], Mark Parrington[4], Sebastien Massart[4], Benjamin Gaubert[5], Youngjae Lee[6], Danbi Kim[6], Jinsang Jung[7], Jinkyu Hong[8], Je-Woo Hong[8], Yugo Kanaya[9], Mindo Lee[6], Ryan M. Stauffer[10,11], Anne M. Thompson[11], James H. Flynn[12], and Jung-Hun Woo[13]

[1]Dept. of Hydrology and Atmospheric Sciences, University of Arizona, Tucson, AZ, USA
[2]NASA Langley Research Center, Hampton, VA, USA
[3]Science Systems and Applications, Inc., Hampton, VA, USA
[4]European Centre for Medium-Range Weather Forecasts, Reading, UK
[5]Atmospheric Chemistry Observations and Modeling Laboratory, National Center for Atmospheric Research, Boulder, CO, USA
[6]National Institute of Environmental Research, Korea
[7]Korea Research Institute of Standards and Science, Korea
[8]Department of Atmospheric Sciences, Yonsei University, Korea
[9]Japan Agency for Marine-Earth Science and Technology, Japan
[10]Universities Space Research Association, Columbia, MD, USA
[11] Earth Sciences Division, NASA Goddard Space Flight Center, Greenbelt, MD, USA
[12]Department of Earth and Atmospheric Sciences, University of Houston, Houston, TX, USA
[13]Dept. of Advanced Technology Fusion, Konkuk University, Korea

Correspondence to: Wenfu Tang (wenfutang@email.arizona.edu)

Atmos. Chem. Phys. Discuss., https://doi.org/10.5194/acp-2018-71
Manuscript under review for journal Atmos. Chem. Phys.
Discussion started: 26 January 2018

Abstract. Accurate and consistent monitoring of anthropogenic combustion is imperative because of its significant health and environmental impacts, especially at city-to-regional scale. Here, we assess the performance of the Copernicus Atmosphere Monitoring Service (CAMS) global prediction system using measurements from aircraft, ground sites, and ships during the Korea United States Air Quality (KORUS-AQ) field study in May to June 2016. Our evaluation focuses on CAMS CO and CO_2 analyses plus two higher resolution forecasts (16-km and 9-km horizontal resolution), to assess their capability in predicting combustion signatures over East Asia. Our results show a slight overestimation of CAMS CO_2 with a mean bias against airborne CO_2 measurements of 2.2, 0.7, and 0.3 ppmv for 16-km and 9-km CO_2 forecasts, and analyses, respectively. The positive CO_2 mean bias in the16-km forecast appears to be consistent across the vertical profile of the measurements. In contrast, we find a moderate underestimation of CAMS CO with an overall bias against airborne CO measurements of -19.2 (16-km), -16.7 (9-km), and -20.7 ppbv (analysis). This negative CO mean bias is mostly seen below 750 hPa for all three forecast/analysis configurations. Despite these biases, CAMS show a remarkable agreement with observed enhancement ratios of CO with CO_2 over Seoul metropolitan and over the West Sea, where East Asian outflows were sampled during the study period. More efficient combustion is observed over Seoul ($\Delta CO/\Delta CO_2$= 9 ppbv/ppmv) compared to the West Sea ($\Delta CO/\Delta CO_2$= 28 ppbv/ppmv). This 'combustion signature contrast' is consistent with previous studies in these two regions. CAMS captured this difference in enhancement ratios (Seoul: 8-12 ppbv/ppmv, West Sea: ~30 ppbv/ppmv) regardless of forecast/analysis configurations. The correlation of CAMS CO bias with CO_2 bias is relatively high over these two regions (Seoul: 0.64-0.90, West Sea: ~0.80) suggesting that the contrast captured by CAMS may be dominated by anthropogenic emission ratios used in CAMS. However, CAMS shows poorer performance in terms of capturing local-to-urban CO and CO_2 variability. Along with measurements at ground sites over the Korean peninsula, CAMS produces too high CO and CO_2 concentrations at the surface with steeper vertical gradients (~0.4 ppmv/hPa for CO_2 and 3.5 ppbv/hPa for CO) in the morning samples than observed (~0.25 ppmv/hPa for CO_2 and 1.7 ppbv/hPa for CO), suggesting weaker boundary layer mixing in the model. Lastly, we find that the combination of CO analyses (i.e., improved initial condition) and use of finer resolution (9-km vs 16-km) generally produce better forecasts.

1. Introduction

Anthropogenic combustion significantly impacts air quality, climate, ecosystem, agriculture, and public health at local to global scales (Charlson et al, 1992; Doney et al., 2007; Feely et al., 2004; Heald et al., 2006; Maher et al., 2016). This is especially the case in megacities where human activities are most intense, accompanied by immense energy consumption, mainly in the form of fossil-fuel combustion, which directly leading to enhanced emissions of air pollutants, greenhouse gases, and waste energy. In particular, cities in the Asian region that are rapidly developing in recent decades are subject to more frequent severe pollution conditions (Yang et al., 2013; Guo et al., 2014; Ohara et al., 2007; Shindell et al., 2008, 2011). It is imperative therefore that we enhance our current capability to monitor, verify, and assess anthropogenic

combustion and its impacts as the number of megacities across the globe is expected to rapidly grow in the following decades (United Nations, 2016). The Copernicus Atmosphere Monitoring Service (CAMS) has a state-of-art global and integrated prediction systems that is currently being implemented to meet this need. The Service is funded by the European Union and it builds upon a legacy of projects such as the Monitoring Atmospheric Composition and Climate (MACC) and GEMS (Hollingsworth et al, 2008).

For nearly a decade, CAMS has been operationally producing daily global near-real time forecasts and analyses of reactive trace gases, greenhouse gases, and aerosols including global reanalyses and estimation of emissions of these atmospheric constituents (Morcrette et al., 2009; Benedetti et al., 2009; Kaiser et al., 2012; Flemming et al., 2015; Flemming et al., 2017; Massart et al., 2016; Agustí-Panareda et al. 2014, Agustí-Panareda et al. 2017). CAMS global forecasts and analyses are based on the Integrated Forecasting System (IFS) of the European Centre for Medium-Range Weather Forecasts (ECMWF), which is also used for Numerical Weather Prediction (NWP). CAMS recently developed 2 forecasts at higher resolution, which have potential advantages compared to lower resolution analysis and/or forecast, in terms of local-to-regional air quality (Table 1).

The Korea United States Air Quality (KORUS-AQ) field measurement campaign offers a unique opportunity to assess the accuracy and consistency of the high resolution forecast and analysis system of CAMS and its skill in simulating atmospheric CO_2 from anthropogenic combustion. During May to June 2016, the KORUS-AQ field collected comprehensive measurements of air quality (including CO_2 and tracers of fossil-fuel combustion) over the South Korean peninsula and its surrounding waters. KORUS-AQ is an international collaboration between U.S. and South Korea to better understand the factors controlling air quality in the region across urban, rural, and coastal interfaces (Kim and Park, 2014, KORUS-AQ White Paper). This field campaign follows several NASA-led sub-orbital missions in the past focusing on air quality in the United States (e.g., DISCOVER-AQ, SEAC^{4}RS), and pollution outflows from Asia (e.g., TRACE-P, INTEX-B, ARCTAS) and integrating the measurements from these campaigns to satellite retrievals and air quality models (Crawford et al., 2014; Toon et al., 2016; Jacob et al., 2003; Singh et al., 2009; Jacob et al., 2010). Local measurements over the West Sea, often representative of Chinese pollution outflow, and over the Seoul metropolitan area provide a rich dataset that is very useful in evaluating global prediction and analysis systems like CAMS at city-to-regional scale.

In this study, we evaluate CAMS forecast and analysis of fossil-fuel combustion signatures over the KORUS-AQ spatial and temporal domain. In particular, we use measurements of the main products of combustion (i.e., CO and CO_2) from the NASA DC-8 aircraft, along with observations from five ground sites, two research ships, and four satellites to assess the capability of CAMS to monitor anthropogenic combustion. Although CAMS CO and CO_2 forecasts and analyses have been evaluated previously (Agustí-Panareda et al., 2014; Agustí-Panareda et al., 2016; Agustí-Panareda et al., 2017; Claeyman et al., 2010; Massart et al., 2016; Flemming et al., 2009; Flemming et al., 2015; Flemming et al., 2017), this study is unique for the following reasons: (1) This study is a joint evaluation of CO and CO_2 species, including their associated enhancement ratios which provide insights on CAMS representation of anthropogenic combustion processes; (2) A focus on megacities provides an important baseline investigation. This is especially the case in East Asia where there is still lack of

detailed information and measurements to constrain emission inventories; (3) KORUS-AQ provides a unique opportunity to evaluate the new high resolution global CAMS forecasts of CO and CO_2 at local-to-regional scale. This paper begins with a brief description of CAMS and KORUS-AQ (Section 2), followed by an evaluation of CAMS with airborne measurements (Section 3) and with ground sites, ships, and satellites (Section 4). We provide a summary of our findings in Section 5.

2. Descriptions of CAMS and KORUS-AQ CO and CO_2

2.1 CAMS CO and CO_2 forecasts and analysis

The Copernicus Atmosphere Monitoring Service (CAMS) has been providing global forecasts and analysis of atmospheric composition on a daily basis at ECMWF for nearly a decade with applications on air quality and monitoring of long-lived greenhouse gases. CAMS uses the Integrated Forecasting System (IFS) for Numerical Weather Prediction (NWP) to assimilate a wealth of meteorological observations plus satellite products of atmospheric composition to produce atmospheric analysis of reactive gases (e.g. CO, O_3, NO_2, SO_2), aerosols and long-lived greenhouse gases (e.g. CO_2, CH_4) on the NWP model grid which are then used as initial conditions to forecast the atmospheric composition with a 5-day lead time. The IFS simulates transport of the chemical species (Flemming et al. 2009, Agusti-Panareda et al. 2017) and includes the on-line integration of modules for atmospheric chemistry (Flemming et al. 2015, 2017) and biogenic CO_2 fluxes from terrestrial vegetation (Boussetta et al., 2013) to model atmospheric composition in conjunction with an assimilation system based on four-dimensional variational (4D-VAR) data assimilation (Rabier et al., 2000). The CAMS global atmospheric analysis and prediction system runs at different resolutions and at a different lag times for the various atmospheric species depending on the use of chemistry in the model and the timeliness of the satellite retrievals used in the analysis. The system providing reactive trace gases and aerosols runs at approximately 40 km horizontal resolution with 60 vertical levels and its analysis is available less than 1-day behind real time. While higher horizontal and vertical resolution is used for the analysis and forecasts of greenhouse gases. The analysis of CO_2 and CH_4 is available at around 40 km in the horizontal and 137 vertical levels. Currently the forecasts of CO_2 and CH_4 have the same resolution as the operational weather forecast at ECMWF (137 levels with 9 km horizontal resolution) but previously their resolution was 16 km (from 2015 to 2016). A CO tracer with simplified chemistry based on a linear CO scheme (Massart et al., 2015) is also available in the high resolution forecast. However, the CO_2 and CH_4 analysis is only available 4-days behind real time as the satellite retrievals are not available closer to real time. Because of this, in the 16km resolution forecast CO_2, CH_4 and linear CO are free running and only the meteorology is initialised with the meteorological operational analysis (see Agusti-Panareda et al. (2014) for further details on free-running forecast configuration). Following a recent improvement in the timeliness of the satellite retrievals, the linear CO is initialised with CO analysis, while CO_2 and CH_4 are initialised with a 4-day forecast from the CO_2 and CH_4 40 km analysis in the 9 km forecasts. In order not to lose the small-scale features in the initialization process, a spectral filter is applied to only adjust the large scales in the initial conditions of the forecast (Massart, 2016, personal communication). Table 1 (as well as Fig. S1) provides a summary of the three CAMS configurations and five resulting CAMS products

evaluated in this paper and Fig. 1 depicts the different vertical and horizontal resolutions used in the different CAMS configurations.

For this study, we focus on evaluating the three CO and CO_2 forecasts and analysis products listed above, namely; CO_2 and CO 16-km forecast (FC16s), analyses (ANs) of CO_2 (at 40 km) and CO (at 80 km), and a relatively recent CAMS 9-km CO_2 and CO forecast product (FC9s) which are initialized from its respective analysis. The FC9s are different from FC16s in terms of both resolution and initialization as described above (e.g. the FC16s are produced from a free-running simulation of CO_2 and CO). The near-real time ANs of CO and CO_2 are also different from FC16s and FC9s as these ANs continuously assimilate satellite retrievals of CO total column from Measurements Of Pollution In The Troposphere (MOPITT V5-TIR) and the Infrared Atmospheric Sounding Interferometer (IASI) (Inness et al., 2015) and column averaged dry-air mole fractions of CO_2 (XCO_2) from the Greenhouse gases Observing Satellite (GOSAT) (Massart et al., 2016). FC9s CO are initialized from MOPITT and IASI CO analysis at a previous time, which are then downscaled from 80 km to 9 km by a spectral filtering scheme. Due to observational and computing constraints, FC9s of CO_2 are initialized and downscaled from a 96-hour forecast of CO_2 initialized by GOSAT analysis 4 days earlier.

The IFS contains several components, including an atmospheric general circulation model, a land surface model, an ocean wave model, an ocean general circulation model, and perturbation models for the data assimilation and forecast (Persson, 2001). Model dynamics and numerical procedures, and physical processes are documented in IFS documentation-Cy43r3 (ECMWF, 2017, https://www.ecmwf.int/search/elibrary/part?title=part&year=2017&secondary_title=IFS). Detailed cloud and precipitation physics of the IFS benefits the calculation of wet deposition (Flemming et al., 2017). As for emissions and surface fluxes, CAMS uses the Global Fire Assimilation System (GFAS) for biomass burning fluxes of CO_2 (Kaiser et al., 2012). CAMS uses the anthropogenic CO_2 fluxes that are based on the annual mean of the Emission Database for Global Atmospheric Research version 4.2 (EDGARv4.2). As the most recent year available for EDGARv4.2 is 2008, estimated and climatological trends are used to extrapolate to the years after 2008. The land vegetation fluxes for CO_2 are calculated online by the carbon module of the land surface model in IFS CTESSEL (Boussetta et al., 2013). A biogenic flux adjustment scheme (BFAS) is employed in CAMS to improve the continental budget of CO_2 fluxes (Agustí-Panareda et al., 2014; Agustí-Panareda et al., 2015; Agustí-Panareda et al., 2016). For CO, CAMS uses anthropogenic and biogenic emissions that are based on the MACC/CityZEN EU projects (MACCity) (Granier et al., 2011), and a climatology of The Model of Emissions of Gases and Aerosols from Nature developed under the MACC (MEGAN-MACC) emission inventories (Sindelarova et al., 2014). GFAS is also used for fire emissions. A linear chemistry scheme is used in FC16s for CO (C-IFS-LINCO) for computationally expediency (Claeyman et al., 2010; Flemming et al., 2012; Massart et al. 2015; Eskes et al., 2017). Key aspects of the three CAMS configurations evaluated in this study are listed in Table 1.

2.2 CO and CO_2 measurements during KORUS-AQ

KORUS-AQ is a comprehensive field campaign based on international collaboration between U.S. and South Korea (https://espo.nasa.gov/korus-aq). The goal is to better understand the factors controlling air quality (AQ) in the region across

urban, rural, and coastal interfaces. The field campaign was conducted over South Korean peninsula and surrounding waters from May to June 2016. South Korean peninsula and its surrounding waters is a desirable region to conduct the campaign because: (1) Korea's urban/rural sectors are distinct, which is advantageous for distinguishing anthropogenic and natural emissions; (2) Korea is embedded in a rapidly changing region; (3) the region allows studies of local versus trans-boundary pollution; and (4) air quality monitoring and ground-based measurements are provided by Korea. AQ measurements (including CO_2) from aircrafts, ships, and ground sites were obtained during this period. The campaign was designed to answer three scientific questions, including (1) what are the challenges and opportunities for satellite observations of air quality; (2) what are the factors governing ozone photochemistry and aerosol evolution; (3) how do model performance and needed improvements to better represent atmospheric composition over Korea and its connection to the larger global atmosphere (Kim and Park, 2014, KORUS-AQ White Paper). Fig. 2 shows the study domain ($30°N - 39°N, 123°E - 133°E$) along with the tracks from DC-8 aircraft flights and research ship deployments. The locations of ground sites are also added in Fig. 2. Satellite retrievals from MOPITT CO and Orbiting Carbon Observatory-2 (OCO-2) CO_2 are shown in Fig. 2 to provide spatial context and coverage of remote sensing measurements during the campaign. All the observational data used in this study are summarized in Table 2.

2.2.1 Airborne CO and CO_2 measurements

We use measurements of CO_2 and CO from the DC-8 aircraft. CO_2 was measured by Atmospheric Vertical Observations of CO_2 in the Earth's Troposphere (AVOCET) using a modified LI-COR model 6252 non-dispersive infrared spectrometer (NDIR). This instrument provides CO_2 concentrations with high precision by sensing the difference in light absorption between the continuously flowing sample and reference gases (Vay et al., 2003, 2011; https://airbornescience.nasa.gov/instrument/AVOCET). CO_2 1 Hz 1σ precision and accuracy are ±0.1 ppm and ±0.25 ppm, respectively. CO was measured by the Differential Absorption CO Measurement (DACOM) instrument via infrared wavelength modulation spectroscopy. The system uses three tunable diode lasers providing 4.7, 4.5, and 3.3 μm radiation for accessing absorption lines of CO, N_2O, and CH_4. The time response for CO measurements is 1 s; the precision is < 1% or 0.1 ppbv; the accuracy is 2% (Warner et al., 2010; https://airbornescience.nasa.gov/instrument/DACOM). Calibrations for both instruments were performed during flight at regular intervals using gas standards traceable to the WMO scale (CO_2: x2012; CO: x2008) and certified by NOAA ESRL. Details about the two instruments are listed in Table 2. Note that we use the 1 min (60 s) merged DC-8 data in this study. The data is available at NASA Langley Research Center archive (www-air.larc.nasa.gov/missions/korus-aq/).

There were 20 formal DC-8 science flights. Note that for time reference, the 'Date' in this paper refers to the day on which the flight started in UTC time instead of Korean local time, unless the term 'Local time' is explicitly used. This 'date' in UTC time is one day ahead of Korea local time as all flights typically start at 8am local time. We also divide the flight measurements into five groups based on the land cover below the flight tracks and types of pollution sources with which they can be broadly associated with. These groups are classified as: Seoul metropolitan, Taehwa, West Sea, Seoul-Jeju jetway and

Seoul-Busan jetway (Please refer to Fig. 2 for an illustration of these flight groups). The Seoul metropolitan represents air samples over the large city of Seoul which can have a dominant signature from anthropogenic combustion processes. On the other hand, Taehwa represents air samples over a forest area near Seoul, which can be influenced by both surface carbon fluxes from the local forest as well as anthropogenic emissions from Seoul. Measurements over the West Sea were designed to capture China pollution outflows. The flight tracks over the West Sea were typically zonal tracks forming a 'wall' between China and Korea (see Fig. 2). These flights are conducted only when a China outflow is expected to be present based on weather and AQ forecasts during the campaign. These measurements enable us to investigate combustion signature from China and differentiate them from Seoul. The Seoul-Jeju jetway and Seoul-Busan jetway groups are two jetway flights on which the DC-8 aircraft frequently obtain measurements. The two jetways are both above the Korean peninsula, connecting Seoul to Jeju and Busan, respectively. Flights over Seoul-Busan jetway is designed to capture activities in forest, rural, and Busan urban regions. The flights in Seoul-Jeju jetway, on the other hand, samples air over local power plants, transported air from the West Sea, and over nearby croplands. We will discuss our evaluation CAMS for each of these five groups in Section 3.

2.2.2 Ground-based CO and CO_2 measurements

Observations from the following ground sites are used for comparison with CAMS CO and CO_2: Baengnyeong, Fukue, Olympic Park, Taehwa, and Yonsei University (see Fig. 2 for the site locations). The sites in Baengnyeong and Taehwa are managed by the National Institute of Environmental Research (NIER). Baengnyeong site is located in less populated Baengnyeong Island, Incheon which is northwest of Seoul. The Fukue site belongs to the Japan Agency for Marine-Earth Science and Technology (JAMSTEC) and is located on remote island of Fukue, Japan. The Olympic Park and Yonsei University sites belong to Korea Research Institute of Standards and Science and Yonsei University, respectively. Both sites are located within the Seoul Metropolitan area. These five ground sites cover different environments, which allows us to differentiate between urban (Olympic Park and Yonsei University) and remote (Baengnyeong and Fukue) air quality conditions during the campaign. The sites in Baengnyeong, Fukue, and Olympic Park provide measurements of CO (in ppbv), while the site in Yonsei University provides measurements of CO_2 (in ppmv). Only the site in Taehwa provides measurements of both CO (in ppbv) and CO_2 (in mg/m^3) (Kim et al., 2013). Locations of the five sites, and corresponding instruments and data intervals are provided in the Table 2. Note that we use data from these sites taken during the KORUS-AQ campaign period to provide the ground context of our evaluation.

2.2.3 Ship observations

We use ship measurements of CO from Jangmok and Onnuri. Both of them are research vessels owned by Korea Institute of Ocean Science and Technology. The ship deployments are part of the Korea-United States Ocean Color (KORUS-OC) field study coinciding with KORUS-AQ. KORUS-OC was led by NASA and the Korean Institute of Ocean Science and Technology, focusing on the ocean color, biology and biogeochemistry as well as atmospheric composition in

coastal waters adjacent to Korea (https://www.asp.ucar.edu/sites/default/files/4_Emmons_07_27_2016.pdf). The two ships sailed along the Korean coast from May 20th to June 5th. Tracks of the two ships are shown in Fig. 2 by dark grey (Jangmok) and light grey (Onnuri). CO measurements in Jangmok and Onnuri were taken from the Thermo 48i-TLE CO analyzer and Thermo 48C CO analyser, respectively (http://www.kiost.ac.kr/kor.do), and are provided every minute.

2.2.4 Satellite-derived CO and CO_2 retrievals

We use four sets of satellite-derived measurements for comparison with CAMS CO and CO_2. We use retrievals of CO_2 column-averaged dry air mole fraction (XCO_2) from NASA OCO-2, version 7, Level 2 (L2) full product with recommended quality control (Crisp et al. 2004; Boesch et al., 2011; Wunch et al. 2011a, b; https://oco.jpl.nasa.gov/). and from Japan Aerospace Exploration Agency (JAXA) GOSAT, Level 2 (L2), version 2 (Yokota et al., 2004, 2009; Morino et al., 2011; Crisp et al. 2012; http://global.jaxa.jp/projects/sat/gosat/). Short-wavelength Infrared observations measured by the Thermal And Near-infrared Sensor for carbon Observation (TANSO) onboard the GOSAT satellite are used to retrieve XCO_2. OCO-2 also has three specific Near Infrared (NIR) wavelength bands to retrieve XCO_2 (https://oco.jpl.nasa.gov/). For CO, we use the NASA Terra MOPITT version 6, Level 2, multispectral (Thermal Infrared/Near Infrared; TIR/NIR) total column retrievals (MOP02J, L2, V6) with recommended quality control. Compared to thermal infrared only retrievals (TIR), these retrievals have an enhanced sensitivity to the lower tropospheric CO (Deeter et al., 2014; https://www2.acom.ucar.edu/mopitt). In addition, we also use total column mole fractions of CO from IASI, Level 2 data with recommended quality control (George et al., 2009; Clerbaux et al., 2009). IASI is on board MetOp-A and B satellites and uses Fast Optimal Retrievals on Layers for IASI (FORLI) to retrieve CO distributions from the thermal infrared (TIR) spectra. We applied the associated averaging kernels from MOPITT and IASI to CAMS CO before comparison as these retrievals exhibit large sensitivities in the free troposphere. We also note that both IASI and MOPITT have significantly more observations than OCO-2 and GOSAT. As summarized in Table 2, resolutions of OCO-2, GOSAT, MOPITT, and IASI are 2.25×1.29 km, 10.5×10.5 km, 22×22 km, and 12×12 km, respectively. The revisit times for the four satellites are also different. OCO-2 overpasses at 1:18 - 1:33 pm, GOSAT overpasses at around 1 pm. Revisit time is 10:30 am for MOPITT, and 9:30 am for IASI. Uncertainties have also been reported for these satellite products. OCO-2 XCO_2 has uncertainties of 1-2 ppm (Boesch et al., 2011) while GOSAT XCO_2 has retrieval errors of 2 ppm (Griffith et al. 2011; Crisp et al. 2012). Deeter et al. (2014) reported 0.09e18 molecules/cm^2 for total column retrieval for MOPITT. Wachter et al. (2012) reported uncertainties to be <13% for IASI FORLI.

3. Comparison with airborne measurements

Here, we evaluate CAMS forecasts and analysis of CO and CO_2 with NASA DC-8 aircraft observations. We interpolate the 4-D fields of CAMS CO and CO_2 model output to collocate with flight measurements in both space and time. The equivalent model data for all flights and for the three configurations (FC16s, FC9s, ANs) are made available in the same file format as the 1-min merged DC-8 dataset to facilitate model to observation comparison. We also estimate enhancement

ratios of CO and CO_2 from both airborne and model data and analyse its spatial and temporal variations across different flights. We present in the following subsections the summary statistics of our comparison of CAMS data with DC-8.

3.1 Performance across all flights

Across all flight data, CAMS overestimates CO_2, with mean biases of 2.2, 0.7, and 0.3 ppmv for FC16s, FC9s, and ANs, respectively. As found by Agusti-Panareda et al (2016), the overall overestimation of CO_2 associated with the biogenic bias correction. In contrast, CAMS underestimates CO with mean biases for FC16s, FC9s, and ANs against DC-8 of -19.2, -16.7, and -20.7 ppbv, respectively. The mean bias is calculated as the average across all data of CAMS minus DC-8. We also find that the overall pairwise correlation between DC-8 and CAMS is moderately high (CO_2: 0.52 to 0.57, CO: 0.65–0.73) while the root-mean-square-errors (RMSEs) in CAMS relative to DC-8 are about 7 ppmv for CO_2 and 80 ppbv for CO. These statistics can be summarized using a Taylor diagram as shown in Fig. S2 and Fig. S3 of the supplementary material. We also calculated the associated Taylor scores to summarize the skill of CAMS in capturing the observed CO_2 or CO variations (please refer to Equation S1 in the supplement). We find that CAMS have relatively good skill regardless of configuration: for CO_2, the skill scores are 0.82 (FC16s), 0.82 (FC9s), and 0.75 (ANs); while for CO, the skill scores are 0.85 (FC16s), 0.86 (FC9s), and 0.83 (ANs). However, it is important to note that these statistics can vary from flight to flight and the skill for CO_2 is not necessarily related to those for CO. For instance, for the May 10th flight, where a southern peninsula outflow was expected, CAMS ANs show higher skill than those from FC9s in terms of both CO_2 and CO, while the scores of FC16s are higher than those of FC9s in terms of CO (Fig. S4). Yet, for the May 3rd flight, where a weak Chinese influence was expected, the scores of FC16s and FC9s are higher for CO_2 than CO, while we find the opposite for the June 2nd flight, where DC-8 sampled local influences. Lastly, we note that the skill of CAMS during the June 4th flight is not high for either species. This flight was designed to measure local point sources with large variations at much finer scales.

3.2 Performance across individual flights

We present in Fig. 3 the summary statistics of CAMS against DC-8 measurements for all 20 individual flights. This is shown in the second to fourth rows of Fig. 3 as boxplots of the bias for FC16s, ANs and FC9s, respectively. We also show the boxplot of DC-8 CO_2 (first row left column) and CO (first row right column) for each flight as points of comparison. The overall mean, median, interquantile range (IQR), and standard deviation (sigma) of DC-8 CO_2 mixing ratios (in ppmv) are 410.37, 408.25, 5.97, and 7.73 respectively. The overall mixing ratio, which varies within 1 to 2 percent, are slightly higher than the month median observed in Mauna Loa (NOAA https://www.esrl.noaa.gov/gmd/ccgg) for May 2016 (408±1 ppmv). For DC-8 CO mixing ratios (in ppbv), the corresponding statistics (mean: 204.59, median:183.90, IQR:127.97, sigma: 101.74) show enhanced CO (and larger variance) than the background value observed in Mauna Loa (100±24 ppbv). In general, CAMS overestimates CO_2 and underestimates CO for most flights. Differences also exist among the 20 flights in terms of both DC-8 measured mixing ratios and model biases. For flights with higher observed variances, CAMS biases and the corresponding variance of the biases tend to be also larger. This is related to variations in weather conditions during the

campaign along with variations in sampling goals of the science flights. For example, the flights in May 3rd, May 17th, May 24th, May 29th, and May 30th were specifically designed to capture Chinese pollution outflow. In these days, the variances in CAMS biases for CO (but not CO_2) are larger than the average. The colored shades in Fig. 3 indicate flights for 'special conditions'. The grey and yellow shades indicate two special cases that we study in detail in later sections. In particular, DC-8 flew a 'wall' over the West Sea on May 24th to investigate the transport of Chinese pollution. On June 4th, DC-8 flew near Seoul to measure pollution from local point sources (e.g., power plants). The other shades indicate that the flights were conducted during a frontal passage (purple) and that the flights may possibly be affected by fires in Siberia (orange). These flights were not further analyzed in this study since for example the May 26th flight (with frontal passage influence) and the May 17th and May 19th flights (with possible fire influence) do not clearly stand out from the other flights (see Fig. 3).

3.3 Performance across flight groups

Here, we evaluate CAMS per flight group as described in section 2.2.1. We show in Fig. 4 the probability density functions (pdfs) of CO and CO_2 for DC-8 and CAMS per flight group. The pdf of CAMS CO_2 (which exhibits a longer tale to higher values) show a general offset to higher values relative to DC-8 (except for West Sea). There is a systematic overestimation of CAMS CO_2 against DC-8. Accordingly, the 'apparent local background' of CO_2 (lower tales of the pdf) is relatively high in CAMS than DC-8. In contrast, CO is underestimated in CAMS across all of the five groups. The pdfs of CO in CAMS show a bi-modal distribution (except in Taehwa and West Sea) indicative of two dominant AQ conditions sampled by DC-8 over this region. The shapes of the CO pdfs in CAMS largely differs from DC-8 (except in Taehwa). We see a higher frequency of occurrence of the two to three modes in West Sea in CAMS that is not apparent in DC-8 while the opposite is the case in Seoul-Busan. This suggests that the underestimation of CO in CAMS may not be systematic or may be caused by biases in CO background values. The pdf over the West Sea also show that CAMS underestimates (or even misses) the more elevated CO observed in DC-8.

We further investigate the differences between CAMS and DC-8 by looking at the bias in the mean profiles. We show in Fig. 5 the mean profiles for all data and each individual group. We find that the overall bias in CAMS CO_2 is systematic and close to uniform across all layers (FC16s: ~2.2 ppmv, FC9s: ~1 ppmv, and ANs: ~0.8 ppmv). This overestimation is true for all flight groups except over West Sea. On the other hand, for CO, the overall bias in CAMS is mostly evident in the lower troposphere (about -20 to 25 ppbv below 700 hPa). This underestimation is especially the case over the West Sea and is consistent with the pdfs in Fig. 4.

3.3.1 Seoul metropolitan and Taehwa

The airborne measurements over the Seoul metropolitan area were mostly during frequent aborted landing maneuvers (i.e. missed approaches) over Seoul air base. More than 90% of the measurements in this group are taken below 850 hPa. Fig. 4 shows that the performance of FC16s, FC9s, and ANs are alike over Seoul for both CO and CO_2, in contrast to the other four flight groups. Given that the measurements over Seoul are dominated by boundary layer and anthropogenic

emissions in Seoul, the model performance over Seoul are most likely to be driven by local emissions. We show in Fig. 6 the mean vertical profiles over Seoul below 800hPa. For CO_2, FC9s profiles agree well with the observations. This is not the case for CO, where FC16s, FC9s, and ANs do not agree well with DC-8, but with the bias in ANs being relatively smaller. However, the near surface temporal variations (changes in the profile from morning to afternoon) observed by DC-8 are captured by FC16s, FC9s, and ANs. It is worth noting that over Seoul, there is an abrupt change in the profile at around 925 hPa for both CO and CO_2 of the morning samples. Accordingly, CO is overestimated below 925 hPa and underestimated above 925 hPa. This vertical gradient (i.e., change in mixing ratios divided by change in pressure) in the morning samples of DC-8 CO_2 and CO are about 0.25 ppmv/hPa and 1.7 ppbv/hPa, respectively. In contrast, the gradients of CO_2 in CAMS are 0.50 ppmv/hPa for FC16s, 0.34 ppmv/hPa for FC9s, and 0.45 ppmv/hPa for ANs while the gradients of CO in CAMS are 4.2 ppbv/hPa for FC16s, 3.4 ppbv/hPa for FC9s, and 3.3 for ANs. It is evident that these gradients (CO and CO_2) regardless of CAMS configuration are significantly steeper than observed. While in part this may be attributed to overestimation of emissions during rush hours (and night-time) in Seoul along with model representativeness errors in the boundary layer, we attribute this steep gradient to a possible weaker boundary layer mixing in CAMS since there is an important contrast between near surface CO (overestimation) and CO aloft (underestimation) which cannot be explained by emissions alone. This is not very apparent in CO_2 since there is an overestimation of background CO_2 superimposed on this difference.

In Taehwa, the differences between morning and afternoon samples are not as large compared to Seoul metropolitan. The CO_2 profiles from ANs and FC9s are apparently closer to DC-8 than from FC16s. However, this difference is not obvious for the CO profiles. Note that in the afternoon (2-4pm), measured CO_2 mixing ratio near surface (at 975 hPa) becomes lower than the layer above, indicating a possible drawdown of CO_2 by underlying vegetation in Taehwa. This change is captured by CAMS, especially in FC9s.

3.3.2 West Sea

As previously mentioned, the flights over the West Sea are focused on capturing pollution outflow from China. Both CO and CO_2 in this flight group are underestimated by CAMS below 900 hPa (Fig. 5). It is the only group in which near surface CO_2 is underestimated by all the three CAMS configuration. In addition, the underestimation of CAMS CO over the West Sea is more significant than that over the other groups. We list two possible reasons for this unique model performance over the West Sea considering that the Chinese outflows constitute the dominant influence of CO and CO_2 samples in this group. First, the transport of surface pollution from China to the West Sea is not well represented in CAMS. Second, emissions in China may not be as well quantified than in Korea. During the May 24th flight, a strong outflow from China was expected, so DC-8 aircraft flew an extended sampling "wall" over the West Sea to sample transport from China. We show in Fig. 7 some of the details of this flight. In particular, we show the vertical cross sections of meridional (panel a) and zonal (panel b) fluxes of CO and CO_2 in CAMS FC9s. These fluxes are calculated as the product of meridional (from west to east) or zonal (from south to north) wind speed with simulated species density (i.e. in terms of units, $\frac{\mathrm{m}}{\mathrm{s}} \times \frac{\mathrm{kg}}{\mathrm{m}^3} = \frac{kg}{m^2 \cdot s}$).

The China outflow moving towards West Sea and Seoul is well demonstrated in the fluxes of CO in panel (a) and (b) especially in the region marked by the black rectangles. This outflow is not apparent in the fluxes of CO_2. This is because the variations in CO_2 density are very low relative to CO_2 background in contrast to CO variations. Hence, the wind speeds dominate the transport flux variations in CO_2. We also show in Fig. 7 panel (c) the measurements of DC-8 aircraft and the bias of FC9s over the West Sea on that day. As can be seen in Fig. 7, CAMS CO_2 and CO are largely underestimated (CO_2: 2-4 ppmv, CO: 86-88 ppbv) for this flight. This underestimation in both species is consistent with Fig. 5. Note that the underestimation of CO_2 over the West Sea is not consistent with other flights and the overall results. This underestimation could be associated with an underestimation of anthropogenic emissions in China, and/or transport from China to the West Sea. This is discussed in Section 3.4 in more details. In summary, the transport pattern of China outflow (CO and CO_2) to the West Sea is captured but the abundances of both CO and CO_2 are underestimated by CAMS especially near the surface.

3.3.3 Seoul-Jeju and Seoul-Busan jetways

Measurements in the Seoul-Jeju and Seoul-Busan jetways are both above the South Korean peninsula, connecting Seoul to Jeju and Busan, respectively. While both flight groups share some common features, they are treated here as two distinct groups for the following reasons: (1) Seoul-Jeju jetway is close to the west coast of South Korea, whereas Seoul-Busan jetway sampled air southeast of Seoul and more inland; (2) There are more croplands, urban, and build-up areas along Seoul-Jeju jetway while there are more forested areas along Seoul-Busan jetway; (3) There are some important point sources along Seoul-Jeju jetway such as power plants and the Daesan chemical facility. In fact, the June 4th flight was designed to survey point sources west of Seoul and focused more to the Seoul-Jeju jetway. Details of the June 4th flight are summarized in Fig. 8. In contrast to the overall statistics across all flight groups, FC16s, FC9s, and ANs for this flight clearly overestimate CO near point sources. We also note that measurements for this flight are mostly taken below 900 hPa. As such, the spatial variations are larger near point sources than in other conditions. Nevertheless, these variations are not well captured by CAMS, especially by ANs. This may be due to its coarser grid representation (i.e., 40 km for CO_2 and 80 km for CO). In addition, we find a difference in terms of mean bias in CO_2 between CAMS FC9s and FC16s. This difference is not apparent in CO. This implies there might be large spatiotemporal errors existing in CO emission inventories in the region, since higher emission resolution does not result in an improvement. In this case, increasing the spatiotemporal resolution might even weaken the simulation results, whereas lower resolution usually agrees better with observations as it "diffuses" the error of the emissions.

3.4 Enhancement ratios of CO to CO_2

We also evaluate the three CAMS configuration against DC-8 in terms of enhancement ratios of CO to CO_2 for all flights and for each flight group. We conduct a reduced major axis (RMA) regression to estimate the sensitivity of CO to CO_2 ($\Delta CO/\Delta CO_2$) with the 1 minute merges. We use RMA instead of ordinary least squares (OLS) regression as the two variables (CO and CO_2) are both subject to error (Smith, 2009). The slope estimate in the RMA corresponds to enhancement

ratio of CO and CO_2. This ratio can reflect the emission ratios of a particular area especially when using near field data (Parrish et al. 2002). Such analysis has been used in previous studies for surface CO and NO_X (Parrish et al. 2002), flask samples of CO and CO_2 in East Asia (Turnbull et al., 2011), airborne measurements of CO and CO_2 during TRACE-P (Suntharalingam et al. 2004), surface CO and CO_2 in rural Beijing (Wang et al. 2010) and more recently with satellite retrievals of CO (MOPITT) and CO_2 (GOSAT) (Silva et al., 2013). We present our estimates of $\Delta CO/\Delta CO_2$ (with units of ppbv/ppmv) from DC-8 and CAMS FC16s, FC9s and ANs in Table 3. Overall, the observed $\Delta CO/\Delta CO_2$ during the KORUS-AQ campaign is ~13 ppbv/ppmv (or ~1.3%). This is a relatively low value compared to reported ratios in more polluted megacities such as Beijing. The lowest $\Delta CO/\Delta CO_2$ among the five flight groups is observed over Seoul (~9 ppbv/ppmv). The observed $\Delta CO/\Delta CO_2$ for other groups within Korea ranges from ~10 ppbv/ppmv (Seoul-Jeju) to ~16 ppbv/ppmv (Seoul-Busan and Taehwa). Taehwa is close to and sometimes downwind of Seoul, but has higher observed $\Delta CO/\Delta CO_2$ than Seoul. We attribute this difference to biogenic CO sources and biospheric influence on CO_2 over Taehwa. The highest $\Delta CO/\Delta CO_2$ (~28 ppbv/ppmv) is observed over the West Sea. This ratio is a sharp contrast to Seoul and other flight groups over Korea. This indicates that the bulk combustion efficiency over Seoul is higher in Seoul than in the China pollution outflows over the West Sea. The ratio over the West Sea is very consistent with $\Delta CO/\Delta CO_2$ observed over China (upwind of West Sea) during KORUS-AQ by ARIAs (20-100 ppbv/ppmv (REF). Such 'combustion signature contrast' is consistent with previous studies in the region. During TRACE-P in 2001, the observed ratio over Japan is ~12-17 ppbv/ppmv and ~50-100 ppbv/ppmv over northern China (Suntharalingam et al. 2004). Over Shangdianzi, China and Tae-Ahn Perninsula (TAP), Korea, Turnbull et al. (2011) reported $CO:CO_2$ff ratios (which are derived from measurements of CO and $\Delta^{14}CO_2$ in flask samples taken during winter 2009/2010), of ~47 and ~44 ppbv/ppmv, respectively. They also reported that the South Korea samples from TAP have $CO:CO_2$ff of ~13 ppbv/ppmv. Wang et al. (2010) reported a change in observed $\Delta CO/\Delta CO_2$ near Beijing from 34-42 ppbv/ppmv in 2005-2007 to 22 ppbv/ppmv in 2008. Finally, $\Delta CO/\Delta CO_2$ derived from satellite retrievals in 2010 indicate a similar contrast between Beijing/Tianjin (~25-50 ppbv/ppmv) and Seoul (~7-9 ppbv/ppmv). Despite the differences in the data sources (satellites, airborne measurements, flask samples) and time period, these $\Delta CO/\Delta CO_2$ values are consistent and all point to a 'combustion signature contrast' between Korea and China. We expect that this contrast may be decreasing over time as Chinese combustion activities become more efficient.

These observed ratios are remarkably consistent with $\Delta CO/\Delta CO_2$ from CAMS (see Table 3). The three CAMS configurations have $\Delta CO/\Delta CO_2$ over Seoul metropolitan of ~8 to 12 ppbv/ppmv and over West Sea of ~31-32 ppbv/ppmv. Our rough estimates of CO to CO_2 emission ratios in CAMS over Seoul and China during KORUS-AQ also show marked similarity with CAMS enhancement ratios. The CO to CO_2 emission ratios over China is about 28 (1000 mole/mole) and about 10 (1000 mole/mole) over Korea. Our results suggest that CAMS emission ratios reflect this contrast and that the modeled $\Delta CO/\Delta CO_2$ is indicative of emissions of Seoul and China. To further understand the skill of CAMS in capturing this contrast, we compare the observed correlation between CO and CO_2 and the correlation from CAMS FC16s, FC9s, and ANs. This corr(CO_2,CO) is presented in the second row of Table 3. Over Seoul, the observed corr(CO_2,CO) is moderately high

(~0.8), which is likely driven by common CO and CO_2 sources (mostly local anthropogenic emissions from Seoul). This correlation is well captured by ANs and FC9s but not FC16s. We attribute this difference to a better initialization in ANs and FC9s due to assimilation. The observed corr(CO_2,CO) over the West Sea even higher (0.89), indicating that CO and CO_2 comes from common sources in China. However, this corr(CO_2,CO) is not captured by any of the three configurations (0.25-0.42). A few factors may contribute to this low corr(CO_2,CO) over the West Sea. First, the flight on May 12th is a noteworthy source of low corr(CO_2,CO) in CAMS. We have shown in Fig. 3 that the major goal of this flight is to study AQ conditions during a frontal passage instead of sampling China outflows. Even though part of the track during May 12th is located in the West Sea, the AQ features of that day are evidently different from China outflow events. After excluding measurements during May 12th, the corr(CO_2,CO) in CAMS (FC16s-0.51, FC9s-0.43, and ANs-0.29) are now higher albeit still lower than observed (0.9). Uncertainties in model transport can be a likely cause as the corr(CO_2,CO) can be subject to transport errors even though $\Delta CO/\Delta CO_2$ may not necessarily be affected. Performance of CAMS over Baengnyeong site (discussed in Section 4.1) also implies possible issues with transport of China pollution towards the West Sea. Furthermore, the difference in temporal representation of China emissions in CAMS may contribute to this mismatch in timing and hence resulting to low correlation. As mentioned in Section 2, CAMS uses prescribed monthly emission for CO while the diurnal cycle of CO_2 fluxes is calculated online in CAMS. Lastly, the corr(CO_2,CO) in FC16s and FC9s are closer to observed corr(CO_2,CO) than in ANs suggesting that resolution may also play a role. For the other three flight groups, the observed corr(CO_2,CO) are not as high as those over Seoul and the West Sea. This implies that CO_2 and CO observed over these three flight groups may not come from common sources and/or have been mixed with the environment. CAMS corr(CO_2,CO) do not always agree with observed corr(CO_2,CO). Overall, corr(CO_2,CO) from FC16s is higher than observed while corr(CO_2,CO) from FC9s and ANs agree well with observed corr(CO_2,CO). Again, this may be related to the fact that FC16s comes from a free running simulation (i.e., not initialized with analyses).

Finally, we present the correlation between the biases of CAMS for the two species ($\mathrm{corr}(\mathrm{Bias}_{CO},\mathrm{Bias}_{CO_2})$) (please see the third row of Table 3). This correlation provides another piece of information on whether the performance of CAMS in CO_2 and CO are related. We find that $\mathrm{corr}(\mathrm{Bias}_{CO},\mathrm{Bias}_{CO_2})$ are high over Seoul and the West Sea, indicating that the performance of CAMS in CO and CO_2 are related for the two groups. Over the West Sea, FC16s, FC9s, and ANs perform similarly. However, the $\mathrm{corr}(\mathrm{Bias}_{CO},\mathrm{Bias}_{CO_2})$ are lower in the other three groups relative to Seoul and the West Sea. In addition, our results show that ANs and FC9s usually have lower $\mathrm{corr}(\mathrm{Bias}_{CO},\mathrm{Bias}_{CO_2})$ than FC16s, especially over Seoul. This implies that FC16s performance in CO_2 and CO are more strongly related than in FC9s and ANs performance, which could be associated again with the fact that FC16s comes from a free running simulation while FC9s and ANs are both initialized from analyses. The assimilation of CO and CO_2 satellite retrievals may reduce the interdependence of CAMS CO_2 and CO performance.

Atmos. Chem. Phys. Discuss., https://doi.org/10.5194/acp-2018-71
Manuscript under review for journal Atmos. Chem. Phys.
Discussion started: 26 January 2018

Atmospheric Chemistry and Physics Discussions

4 Comparison with other measurements

In this section, we evaluate CAMS FC16s and FC9s, and ANs against CO and/or CO_2 measurements from five ground sites, two ships, and four satellites. Unlike DC-8, data on CO_2 or CO in these cases may not be jointly available. In particular, each ground site (except Taehwa) only measures one of the two species. The ships also provide measurements for CO only while the four sets of satellite retrievals of CO_2 and CO are from four different instruments on board four different satellites. Therefore, in this section, CO_2 and CO are evaluated separately, and relationships between CO_2 and CO inferred from some of these sites are only indicative of a larger pattern that we see in DC-8.

4.1 Comparison with ground observations

Here, we focus our evaluation on CAMS performance in capturing surface conditions and diurnal cycle of CO_2 and/or CO. Data from the following five ground sites are used in this study: Baengnyeong, Fukue, Olympic Park, Taehwa, and Yonsei University (Fig. 2 and Table 2). It can be seen in Fig. 9 that CO from Olympic park and CO_2 from Yonsei and Taehwa clearly show a diurnal cycle during KORUS-AQ. This feature is well captured by CAMS. CO at Taehwa on the other hand, exhibit a very weak diurnal cycle that is not captured by CAMS. At this site, CO in CAMS (especially ANs) shows a strong diurnal cycle. Variations of CO in the remote sites of Baengnyeong and Fukue also appears to be irregular and episodic. Signatures of elevated CO can also be seen at these sites, some of which coinciding with pollution transport from China sampled by DC-8. The mean diurnal cycle for these five ground sites can be found in Fig. S5.

While CAMS is able to get the observed timing of CO_2, the modelled magnitudes of CO_2 (and CO) at these sites from CAMS are too high (especially for the sites in and nearby Seoul). We took the average value across a few layers near the model surface in CAMS to provide a reasonable comparison at these sites. We use model vertical layers below 95% of the model surface pressure (i.e., if surface pressure is 1000hPa, we average the layers below 950 hPa) to account for potential weak boundary layer mixing (especially near source regions). This feature in CAMS has been discussed in section 3.3.1. Since this averaging may introduce errors in our comparison, we only evaluate CAMS in terms of relative patterns (diurnal cycle and spatial variability across sites). Note that CAMS CO and CO_2 along the shop tracks (to be discussed in the succeeding section) are also averaged across a few layers in the same way for consistency. We show in Fig. 9 the summary statistics of the bias in CAMS relative to ground observations. The boxplots show that the variability of model bias in CO is in general smaller for remote sites and larger for the two sites in Seoul metropolitan. The bias in CAMS is also smaller in Fukue than in Baengnyeong, where a larger influence of pollution transport from China is observed but not well captured in CAMS. It is also worth mentioning that relative to other sites, CAMS significantly overestimates both CO and CO_2 at Taehwa. This may be due to the proximity of Taehwa to Seoul. The model grid spacing may not be able to resolve well the subgrid-scale processes (emissions) and variations between Seoul and Taehwa. This overestimation is most apparent in CAMS ANs which has a coarser grid spacing (40 km for CO_2 and 80 km for CO) than FC16s and FC9s. In the case of CO_2 at Yonsei, we find lower bias in CAMS FC9s and ANs than FC16s suggesting improvements of CAMS due to better

initialization.

We take advantage of the location of the sites in Olympic Park (CO) and Yonsei University (CO_2) which are within Seoul metropolitan and the collocated measurements of CO and CO_2 in Taehwa to investigate patterns of ground-based $\Delta CO/\Delta CO_2$ in Seoul and Taehwa. Here, we only discuss observed $\Delta CO/\Delta CO_2$ since the modeled $\Delta CO/\Delta CO_2$ at these ground sites may not be accurate given CAMS issues with vertical mixing near the surface and representativeness errors. Following similar analysis with the DC-8 $\Delta CO/\Delta CO_2$, regressions of CO to CO_2 at these sites can represent emission ratios of CO to CO_2 in Seoul metropolitan. Our estimate of $\Delta CO/\Delta CO_2$ from Olympic Park and Yonsei sites is 11.32 ppbv/ppmv. This is consistent with $\Delta CO/\Delta CO_2$ calculated from DC-8 which sampled air closely above these sites (~9 ppbv/ppmv). Our estimate of $\Delta CO/\Delta CO_2$ from the Taehwa site is 6.57 ppbv/ppmv. This is different from our DC-8 estimate of 15.3 ppbv/ppmv. Unlike Seoul, 70% of DC-8 measurements over Taehwa are taken above 800 hPa, Over Taehwa, airborne $\Delta CO/\Delta CO_2$ varies with altitude from 8.92 ppbv/ppmv below 950 hPa, 10.28 ppbv/ppmv below 900 hPa, and 14.74 ppbv/ppmv above 400 hPa.

4.2 Comparison with ship observations

Two research vessels (Jangmok and Onnuri) were deployed during KORUS-OC. The two ships travelled along the Korean coast and measured CO from May 20th to June 5th (as marked in Fig. 2). Measurements of CO from ships, and biases of CAMS FC16s, ANs, and FC9s are shown in Fig. 10. Note that CAMS values along ship tracks are also averaged across a few layers near surface in the same way CAMS at ground sites were processed. CAMS at three (out of four) ground sites tend to underestimate CO, while CAMS overestimates CO relative to ship measurements. This seems to be inconsistent with our findings with airborne measurements (i.e., CO is underestimated by CAMS at lowermost troposphere (Fig. 5 and Fig. 7). This is likely due to the differences in sampling between the airborne and ship measurements. Over sea, the DC-8 often sampled air from China outflow while the two ships continuously sampled air over the waters regardless of the presence of China outflows. The ship measurements reflect surface conditions over waters which may also be different from what is observed by DC-8 along the vertical profile. This inconsistency is further discussed in the next section with satellite data.

4.3 Comparison with satellite retrievals

The total column dry air mole fractions of CO_2 and CO (XCO_2 and XCO) derived from CAMS are compared here to XCO_2 from OCO-2 and GOSAT, and XCO from MOPITT and IASI. It is worth noting that satellite retrievals may have associated bias and uncertainties, which are generally larger than those of ground and airborne measurements. Slight inconsistencies also exist between MOPITT XCO and IASI XCO (George et al., 2009; 2015). We show in Fig. 11 the spatial distribution of CAMS biases against these retrievals. We also summarize the statistics in Table 4. Overall, ANs tend to agree better with satellite observations than the forecasts. For CO, CAMS XCO tends to be higher than MOPITT but lower than IASI. In addition, CAMS XCO agrees better with MOPITT than IASI. For CO_2, CAMS XCO_2 tend to be higher than GOSAT but lower than OCO-2. FC16s, FC9s, and ANs differ from each other in terms of bias when compared to any of the four satellite retrievals although there is no clear difference in terms of RMSE. For XCO, when compared to MOPITT, ANs

are better than the two forecasts in terms of bias, RMSE, and correlation. When compared to IASI, ANs are better in terms of RMSE and correlation, but not its bias. For XCO_2, ANs do not show improvements from the two forecasts when compared to both OCO-2 and GOSAT retrievals. For both XCO and XCO_2, FC9s is not necessarily better than FC16s. In summary, ANs XCO show better agreement with satellite retrievals but this is not the case for XCO_2. Differences in the resolution and amount of satellite data of XCO and XCO_2 could be two possible causes. The spatial and temporal resolutions of FC16s and FC9s are higher than those of ANs while ANs assimilate observational data from these satellite retrievals (except OCO-2). These two factors compete against each other. Because the size of CO data (13612 retrievals for MOPITT and 25509 for IASI over our study domain during KORUS-AQ) is much larger than that of CO_2 (42 for GOSAT over our domain during KORUS-AQ). This is illustrated in Fig. 10 and listed in Table 4. There are more observational constraints for CO in CAMS resulting to better performance of ANs CO. The opposite is the case for CO_2. The model resolution dominates for CAMS CO_2 performance especially with regards to capturing spatiotemporal variability. Scatter plots of CAMS XCO and XCO_2 against satellite observations are also presented in Fig. S6 of the supplementary material.

We note that CAMS overestimates XCO when compared with MOPITT XCO over the West Sea (Fig. 11). This appears to be contradictory to our conclusions in section 3 and the similar inconsistency also exists when we compare CAMS CO with ship measurements (as mentioned in Section 4.2). To further explain this inconsistency, we compare CAMS FC9s with ship measurements and satellite XCO. Because the West Sea flight group in DC-8 measurements forms a zonal 'wall' and such measurements over the West Sea are only conducted when a China outflow is expected, we separate the days when China outflows are present. The following are the days during the campaign when China outflows were expected to occur and DC-8 flights measured walls over the West Sea: May 3rd, May 17th, May 24th, May 29th, and May 30th On May 3rd, May 17th, May 24th, and May 29th, there are no MOPITT observations over the West Sea (Fig. S7). Therefore, the overall differences between CAMS FC9s and MOPITT observations are driven by the non-outflow days. On May 30th, however, there are MOPITT observations over the West Sea. Unlike the overall picture (Fig. 11), we find that CAMS actually underestimates the outflows over the West Sea on that day, which is consistent with our findings in Section 3. On June 1st (a non-China outflow day), comparison with ship measurements indicates that CAMS FC9s overestimates CO near Korean coast. It is also consistent with MOPITT XCO in June 1st (Fig. S7). This overestimation in CAMS FC9s is also captured in our comparison with Baengnyeong (highlighted by a black box in Fig. 10). We find similar overestimation using CAMS FC16s and ANs. Hence, during 'normal' conditions, CAMS tend to overestimate CO over the West Sea, whereas during China outflow events, CAMS tend to underestimate CO.

5 Discussions and Conclusions

We use measurements from the NASA DC-8 aircraft, five ground sites (Baengnyeong, Fukue, Olympic Park, Taehwa, and Yonsei University), and two ships (Jangmok and Onnuri) during the KORUS-AQ field campaign, along with four sets of satellite retrievals (MOPITT XCO, IASI XCO, OCO-2 XCO_2, and GOSAT XCO_2) to evaluate the capability of a high-resolution global modeling system (CAMS) in simulating anthropogenic combustion. Specifically, we evaluate the

performance of CAMS FC16s, FC9s, and ANs of CO_2, CO, and their relationships. Our assessment of the overall performance of CAMS against DC-8 measurements show that: (1) The nominal background CO_2 in CAMS is slightly overestimated (bias is 2.2 ppmv for FC16s, 0.7 ppmv for FC9s, and 0.3 ppmv for ANs), which is further improved by CO_2 analysis. The overall overestimation of CO_2 might be associated with the biogenic bias correction. On the other hand, CO is generally underestimated by CAMS (bias is -19.2 ppbv for FC16s, -16.7 ppbv for FC9s, and -20.7 ppbv for ANs); and (2) Among the three forecasts/analysis configurations, FC9s are more accurate and consistent overall than FC16s and ANs because of the finer model resolution and improved initialization. While ANs are coarser in resolution, they generally perform better than FC16s as the impact of initialization surpasses the impact of resolution (Fig. S2). We also classify the airborne measurements into five groups based on land cover below the flight tracks and associated pollution sources. While CO_2, CO, and their relationships vary across these five groups, CAMS perform well in terms of simulating regional pattern of anthropogenic combustion. This is because: 1) CAMS simulations of both species have relatively low bias; and 2) CAMS reproduces $\Delta CO/\Delta CO_2$ observed by DC-8. Both CAMS and DC-8 show more efficient combustion (low $\Delta CO/\Delta CO_2$) over Seoul than over the West Sea which is representative of Chinese outflows. Our case study on the May 24th flight over the West Sea indicates that the Chinese outflow is captured by CAMS. However, the modeled CO and CO_2 concentrations are significantly underestimated (by -2 to -4 ppmv for CO_2 and -86 to -88 ppbv) especially within the lowermost troposphere. This suggests that, although CAMS emission ratios are relatively consistent with $\Delta CO/\Delta CO_2$, the absolute magnitude of China emissions are still underestimated. CAMS also show poorer performance at local-to-urban scales as exemplified by our case study in the June 4th flight where larger variations near point sources were not represented in CAMS. Our comparisons with measurements from ground sites and two ships indicate that: (1) the diurnal cycle of CO and CO_2 are stronger over urban environments and such periodic features are reasonably captured by CAMS; (2) vertical mixing near sources (such as Seoul) is too weak in CAMS and needs to be improved; and (3) in some cases, FC9s do not show improvements from FC16s (such as over Seoul and the point sources during the June 4th flight), implying large spatiotemporal errors in emission inventories. In these cases, increasing the spatiotemporal resolution might even weaken the simulation results, whereas lower resolution usually agrees better with observations as it "diffuses" the error of the emissions. We also compared XCO and XCO_2 derived from CAMS to satellite retrievals from four instruments (MOPITT CO, IASI CO, OCO-2 CO_2, and GOSAT CO_2). We find that ANs XCO show better agreement with satellite retrievals compared to the forecasts, while ANs CO_2 is no better than the forecasts. We attribute this contrast to significant differences in the number of XCO and XCO_2 satellite data potentially available for assimilation.

We recognize the following limitations of this work. (1) The temporal distribution of airborne measurements are not completely independent from their spatial distributions. For example, most of the measurements in the West Sea group are conducted before noon, whereas measurements over Seoul-Busan jetway are concentrated in the afternoon. (2) CAMS is only evaluated over South Korean peninsula and surrounding waters during the campaign (May 1st to June 10th). More work is needed to determine if our findings are valid over other regions. For example, Agusti-Panareda et al. (2014) reported the overall overestimation of CO_2 in spring over the whole Northern Hemisphere and it is associated with biogenic flux

correction. (3) Inconsistencies exist even among different satellite products (George et al., 2009; 2015), thus limiting our comparisons with CAMS to relative differences; and 4) Our comparison of CAMS with ground and ship measurements are only qualitative and indicative as CAMS surface concentrations are significantly higher than surface observations and not comparable.

Finally, this study has important implications on the design and implementation of current and future prediction system for atmospheric composition and air quality. Although CAMS captured the regional combustion signatures, it still has difficulty representing the variability at local-to-urban scales even at finer resolution. This suggests both improvements in observational constraints and model representation of relevant processes (e.g., emissions and boundary layer mixing).

Data availability. CAMS 16-km forecasts, and analyses are available online (http://apps.ecmwf.int/datasets/data/cams-nrealtime/levtype=sfc/). CAMS 9-km forecasts are available upon request. Observational data from KORUS-AQ will be open to public soon (https://www-air.larc.nasa.gov/cgi-bin/ArcView/korusaq). All the satellite data used in this study are available online. MOPITT CO and OCO-2 CO_2 can be downloaded at https://reverb.echo.nasa.gov/reverb/. IASI CO can be found at http://ether.ipsl.jussieu.fr/ether/pubipsl/iasi_CO_uk.jsp. GOSAT CO_2 data after 2014 is available at http://www.gosat.nies.go.jp/en/.

Acknowledgements. This work is supported by NASA KORUSAQ NNX16AE16G. We thank the KORUS-AQ team for observational data, the CAMS global production team for the model products of CO and CO_2, MOPITT, IASI, OCO-2, and GOSAT data teams for satellite data. IASI CO is provided by LATMOS/CNRS and ULB. We acknowledge NASA and the OCO-2 project for OCO-2 CO_2 data. The authors thank Dr. Cenlin He for helpful comments on improving the paper. The CAMS data was generated using Copernicus Atmosphere Monitoring Service Information [2016].

References

Agustí-Panareda, A., Massart, S., Chevallier, F., Bousetta, S., Balsamo, G., Beljaars, A., Ciais, P., Deutscher, N. M., Engelen, R., Jones, L. and Kivi, R.: Forecasting global atmospheric CO_2. Atmospheric Chemistry and Physics, 14(21), 11959-11983, 2014.

Agusti-Panareda, A., Monitoring upgrades of analysis/forecast system, MACC-III Deliverable D44.04, June 2015.

Agustí-Panareda, A., Massart, S., Chevallier, F., Balsamo, G., Boussetta, S., Dutra, E., and Beljaars, A.: A biogenic CO 2 flux adjustment scheme for the mitigation of large-scale biases in global atmospheric CO 2 analyses and forecasts. Atmospheric Chemistry and Physics, 16(16), 10399-10418, 2016.

Agusti-Panareda, A., Diamantakis, M., Bayona, V., Klappenbach, F., and Butz, A.: Improving the inter-hemispheric gradient of total column atmospheric CO 2 and CH 4 in simulations with the ECMWF semi-Lagrangian atmospheric global model. Geoscientific Model Development, 10(1), 1, 2017.

Andreae, M. O., and Merlet, P.: Emission of trace gases and aerosols from biomass burning. Global biogeochemical cycles, 15(4), 955-966, 2001.

Benedetti, A., Morcrette, J.J., Boucher, O., Dethof, A., Engelen, R.J., Fisher, M., Flentje, H., Huneeus, N., Jones, L., Kaiser, J.W. and Kinne, S.: Aerosol analysis and forecast in the European centre for medium-range weather forecasts integrated forecast system: 2. Data assimilation. Journal of Geophysical Research: Atmospheres, 114(D13), 2009.

Boesch, H., Baker, D., Connor, B., Crisp, D., and Miller, C.: Global characterization of CO2 column retrievals from shortwave-infrared satellite observations of the Orbiting Carbon Observatory-2 mission. Remote Sensing, 3(2), 270-304, 2011.

Boussetta, S., Balsamo, G., Beljaars, A., Panareda, A. A., Calvet, J. C., Jacobs, C., Hurk, B., Viterbo, P., Lafont, S., Dutra, E. and Jarlan, L. (2013). Natural land carbon dioxide exchanges in the ECMWF Integrated Forecasting System: Implementation and offline validation. Journal of Geophysical Research: Atmospheres, 118(12), 5923-5946.

Charlson, R. J., and Schwartz, S. E: Climate forcing by anthropogenic aerosols. Science, 255(5043), 423, 1992.

Claeyman, M., Attié, J. L., El Amraoui, L., Cariolle, D., Peuch, V. H., Teyssèdre, H., Josse, B., Ricaud, P., Massart, S., Piacentini, A. and Cammas, J. P.: A linear CO chemistry parameterization in a chemistry-transport model: evaluation and application to data assimilation. Atmospheric Chemistry and Physics, 10(13), 6097, 2010.

Clerbaux, C., Boynard, A., Clarisse, L., George, M., Hadji-Lazaro, J., Herbin, H., Hurtmans, D., Pommier, M., Razavi, A., Turquety, S. and Wespes, C. (2009). Monitoring of atmospheric composition using the thermal infrared IASI/MetOp sounder. Atmospheric Chemistry and Physics, 9(16), 6041-6054.

Crawford, J.H. and Pickering, K.E.: DISCOVER-AQ: Advancing strategies for air quality observations in the next decade. Environ. Manage, pp.4-7, 2014.

Crisp, D., Atlas, R.M., Breon, F.M., Brown, L.R., Burrows, J.P., Ciais, P., Connor, B.J., Doney, S.C., Fung, I.Y., Jacob, D.J. and Miller, C.E.: The orbiting carbon observatory (OCO) mission. Advances in Space Research, 34(4), pp.700-709, 2004.

Crisp, D., Fisher, B., O'Dell, C., Frankenberg, C., Basilio, R., Bosch, H., Brown, L. R., Castano, R., Connor, B., Deutscher, N. M. and Eldering, A.: The ACOS CO2 retrieval algorithm-Part II: Global XCO2 data characterization, 2012.

Deeter, M. N., Martínez-Alonso, S., Edwards, D. P., Emmons, L. K., Gille, J. C., Worden, H. M., Sweeney, C., Pittman, J.V., Daube, B.C. and Wofsy, S. C.: The MOPITT Version 6 product: algorithm enhancements and validation. Atmospheric Measurement Techniques, 7(11), 3623-3632, 2014.

Doney, S. C., Mahowald, N., Lima, I., Feely, R. A., Mackenzie, F. T., Lamarque, J. F., and Rasch, P. J.: Impact of anthropogenic atmospheric nitrogen and sulfur deposition on ocean acidification and the inorganic carbon system. Proceedings of the National Academy of Sciences, 104(37), 14580-14585, 2007.

ECMWF: IFS Documentation CY43R3. European Centre for Medium-Range Weather Forecasts: Reading, UK, 2017.

Eskes, H.J., Wagner, A., Schulz, M., Christophe, Y., Ramonet, M., Basart, S., Benedictow, A., Blechschmidt, A.-M., Chabrillat, S., Clark, H., Cuevas, E., Flentje, H., Hansen, K.M., Im, U., Kapsomenakis, J., Langerock, B., Petersen, K., Richter, A., Sudarchikova, N., Thouret, V., Warneke, T., Zerefos, C.: Validation report of the CAMS near-real-time global atmospheric composition service: Period June - August 2017. Copernicus Atmosphere Monitoring Service (Cams) Report, Cams84_2015sc2_D84.1.1.7_2017djf_V1.Pdf, May 2017.

Feely, R. A., Sabine, C. L., Lee, K., Berelson, W., Kleypas, J., Fabry, V. J., and Millero, F. J.: Impact of anthropogenic CO2 on the CaCO3 system in the oceans. Science, 305(5682), 362-366, 2004.

Flemming, J., Inness, A., Flentje, H., Huijnen, V., Moinat, P., Schultz, M. G., and Stein, O.: Coupling global chemistry transport models to ECMWF's integrated forecast system. Geoscientific Model Development, 2, 253-265, 2009.

Flemming, J., Peuch, V. H., Engelen, R., and Kaiser, J. W.: A European global-to-regional air pollution forecasting system that combines modeling with satellite observations. EM Magazine, November, 610, 2013.

Flemming, J., Huijnen, V., Arteta, J., Bechtold, P., Beljaars, A., Blechschmidt, A. M., Diamantakis, M., Engelen, R. J., Gaudel, A., Inness, A. and Jones, L.: Tropospheric chemistry in the Integrated Forecasting System of ECMWF. Geoscientific model development, 8(4), 975-1003, 2015.

Flemming, J., Benedetti, A., Inness, A., Engelen, R. J., Jones, L., Huijnen, V., Remy, S., Parrington, M., Suttie, M., Bozzo, A. and Peuch, V. H.: The CAMS interim Reanalysis of Carbon Monoxide, Ozone and Aerosol for 2003–2015. Atmospheric Chemistry and Physics, 17(3), 1945-1983, 2017.

Gamnitzer, U., Karstens, U., Kromer, B., Neubert, R. E., Meijer, H. A., Schroeder, H., and Levin, I.: Carbon monoxide: A quantitative tracer for fossil fuel CO_2? Journal of Geophysical Research: Atmospheres, 111(D22), 2006.

George, M., Clerbaux, C., Hurtmans, D., Turquety, S., Coheur, P. F., Pommier, M., Hadji-Lazaro, J., Edwards, D. P., Worden, H., Luo, M. and Rinsland, C.: Carbon monoxide distributions from the IASI/METOP mission: evaluation with other space-borne remote sensors. Atmospheric chemistry and physics, 9(21), 8317-8330, 2009.

George, M., Clerbaux, C., Bouarar, I., Coheur, P.F., Deeter, M.N., Edwards, D.P., Francis, G., Gille, J.C., Hadji-Lazaro, J., Hurtmans, D. and Inness, A.: An examination of the long-term CO records from MOPITT and IASI: comparison of retrieval methodology. Atmospheric Measurement Techniques, 8, pp.4313-4328, 2015.

Granier, C. et al.: Evolution of anthropogenic and biomass burning emissions of air pollutants at global and regional scales during the 1980–2010 period. Climatic Change (109), 2011.

Griffith, D. W., Toon, G. C., Connor, B., Sussmann, R., Warneke, T., Deutscher, N. M., Wennberg, P.O., Notholt, J., Sherlock, V., Robinson, J. and Uchino, O.: Preliminary validation of column-averaged volume mixing ratios of carbon dioxide and methane retrieved from GOSAT short-wavelength infrared spectra, 2011.

Guan, D., Liu, Z., Geng, Y., Lindner, S. and Hubacek, K.: The gigatonne gap in China/'s carbon dioxide inventories. Nature Climate Change, 2(9), pp.672-675, 2012.

Guo, S., Hu, M., Zamora, M. L., Peng, J., Shang, D., Zheng, J., Du, Z., Wu, Z., Shao, M., Zeng, L. and Molina, M. J. (2014). Elucidating severe urban haze formation in China. Proceedings of the National Academy of Sciences, 111(49), 17373-17378.

Heald, C. L., Jacob, D. J., Park, R. J., Alexander, B., Fairlie, T. D., Yantosca, R. M., and Chu, D. A.: Transpacific transport of Asian anthropogenic aerosols and its impact on surface air quality in the United States. Journal of Geophysical Research: Atmospheres, 111(D14), 2006.

Hollingsworth, A., Engelen, R. J., Benedetti, A., Dethof, A., Flemming, J., Kaiser, J. W., Morcrette, J.J., Simmons, A.J., Textor, C., Boucher, O. and Chevallier, F.: Toward a monitoring and forecasting system for atmospheric composition: The GEMS project. Bulletin of the American Meteorological Society, 89(8), 1147-1164, 2008.

Jacob, D. J., Crawford, J. H., Kleb, M. M., Connors, V. S., Bendura, R. J., Raper, J. L., Sachse, G.W., Gille, J.C., Emmons, L. and Heald, C. L.: Transport and Chemical Evolution over the Pacific (TRACE-P) aircraft mission: Design, execution, and first results. Journal of Geophysical Research: Atmospheres, 108(D20), 2003.

Jacob, D. J., Crawford, J. H., Maring, H., Clarke, A. D., Dibb, J. E., Emmons, L. K., Ferrare, R. A., Hostetler, C. A., Russell, P. B., Singh, H. B. and Thompson, A. M.: The Arctic Research of the Composition of the Troposphere from Aircraft and Satellites (ARCTAS) mission: design, execution, and first results. Atmospheric Chemistry and Physics, 10(11), 5191-5212, 2010.

Kaiser, J.W., Heil, A., Andreae, M.O., Benedetti, A., Chubarova, N., Jones, L., Morcrette, J.J., Razinger, M., Schultz, M.G., Suttie, M. and Van Der Werf, G.R.: Biomass burning emissions estimated with a global fire assimilation system based on observed fire radiative power. Biogeosciences, 9(1), p.527, 2012.

Kim, S., and Park, R. KORUS-AQ: An International Cooperative Air Quality Field Study in Korea, the KORUS-AQ white paper, 2014.

Maher, B. A., Ahmed, I. A., Karloukovski, V., MacLaren, D. A., Foulds, P. G., Allsop, D., Mann, D. M., Torres-Jardón, R. and Calderon-Garciduenas, L.: Magnetite pollution nanoparticles in the human brain. Proceedings of the National Academy of Sciences, 113(39), 10797-10801, 2016.

Massart, Flemming J., Cariolle, D., Jones,L.: High resolution CO tracer forecasts, MACC-III Deliverable D022.04, 2015.

Massart, S., Agustí-Panareda, A., Heymann, J., Buchwitz, M., Chevallier, F., Reuter, M., Hilker, M., Burrows, J. P., Deutscher, N. M., Feist, D. G. and Hase, F.: Ability of the 4-D-Var analysis of the GOSAT BESD XCO 2 retrievals to characterize atmospheric CO 2 at large and synoptic scales. Atmospheric Chemistry and Physics, 16(3), 1653-1671, 2016.

Morcrette, J.J., Boucher, O., Jones, L., Salmond, D., Bechtold, P., Beljaars, A., Benedetti, A., Bonet, A., Kaiser, J.W., Razinger, M. and Schulz, M.: Aerosol analysis and forecast in the European Centre for medium-range weather forecasts integrated forecast system: Forward modeling. Journal of Geophysical Research: Atmospheres, 114(D6), 2009.

Morino, I., Uchino, O., Inoue, M., Yoshida, Y., Yokota, T., Wennberg, P., Toon, G.C., Wunch, D., Roehl, C.M., Notholt, J. and Warneke, T.: Preliminary validation of column-averaged volume mixing ratios of carbon dioxide and methane retrieved from GOSAT short-wavelength infrared spectra, 2011.

Ohara, T. A. H. K., Akimoto, H., Kurokawa, J. I., Horii, N., Yamaji, K., Yan, X., and Hayasaka, T.: An Asian emission inventory of anthropogenic emission sources for the period 1980–2020. Atmospheric Chemistry and Physics, 7(16), 4419-4444, 2007.

Parrish, D. D., Trainer, M., Hereid, D., Williams, E. J., Olszyna, K. J., Harley, R. A., Meagher, J. F. and Fehsenfeld, F. C.: Decadal change in carbon monoxide to nitrogen oxide ratio in US vehicular emissions. Journal of Geophysical Research: Atmospheres, 107(D12), 2002.

Persson, A. User Guide to ECMWF forecast products, 2001.

Rabier F, Jarvinen H, Klinker E, Mahfouf J-F, Simmons, A.: The ECMWF operational implementation of four-dimensional variational assimilation. I: Experimental results with simplified physics. Q. J. R. Meteorol. Soc. 126, 1143 – 1170, 2000.

Shindell, D., Faluvegi, G., Walsh, M., Anenberg, S. C., Van Dingenen, R., Muller, N. Z., Austin, J., Koch, D. and Milly, G.: Climate, health, agricultural and economic impacts of tighter vehicle-emission standards. Nature Climate Change, 1(1), 59-66, 2011.

Shindell, D., Lamarque, J. F., Unger, N., Koch, D., Faluvegi, G., Bauer, S., Ammann, M., Cofala, J. and Teich, H.: Climate forcing and air quality change due to regional emissions reductions by economic sector. Atmospheric Chemistry and Physics, 8(23), 7101-7113, 2008.

Silva, S. J., Arellano, A. F., and Worden, H.: Toward anthropogenic combustion emission constraints from space-based analysis of urban CO_2/CO sensitivity, Geophys. Res. Lett., 40, 4971–4976, doi:10.1002/grl.50954, 2013.

Singh, H. B., Brune, W. H., Crawford, J. H., Flocke, F., and Jacob, D. J.: Chemistry and transport of pollution over the Gulf of Mexico and the Pacific: spring 2006 INTEX-B campaign overview and first results. Atmospheric Chemistry and Physics, 9(7), 2301-2318, 2009.

Sindelarova, K., Granier, C., Bouarar, I., Guenther, A., Tilmes, S., Stavrakou, T., Müller, J.-F., Kuhn, U., Stefani, P., and Knorr, W.: Global data set of biogenic VOC emissions calculated by the MEGAN model over the last 30 years, Atmos. Chem. Phys., 14, 9317-9341, doi:10.5194/acp-14-9317-2014, 2014.

Smith, R.J.: Use and misuse of the reduced major axis for line-fitting. American journal of physical anthropology, 140(3), pp.476-486, 2009.

Streets, D.G., Bond, T.C., Carmichael, G.R., Fernandes, S.D., Fu, Q., He, D., Klimont, Z., Nelson, S.M., Tsai, N.Y., Wang, M.Q. and Woo, J.H.: An inventory of gaseous and primary aerosol emissions in Asia in the year 2000. Journal of Geophysical Research: Atmospheres, 108(D21), 2003.

Streets, D.G., Zhang, Q., Wang, L., He, K., Hao, J., Wu, Y., Tang, Y. and Carmichael, G.R.: Revisiting China's CO emissions after the transport and chemical evolution over the Pacific (TRACE-P) mission: synthesis of inventories, atmospheric modeling, and observations. Journal of Geophysical Research: Atmospheres, 111(D14), 2006.

Taylor, K. E.: Summarizing multiple aspects of model performance in a single diagram. Journal of Geophysical Research: Atmospheres, 106(D7), 7183-7192, 2001.

Toon, O.B., Maring, H., Dibb, J., Ferrare, R., Jacob, D.J., Jensen, E.J., Luo, Z.J., Mace, G.G., Pan, L.L., Pfister, L. and Rosenlof, K.H.: Planning, implementation, and scientific goals of the Studies of Emissions and Atmospheric Composition, Clouds and Climate Coupling by Regional Surveys (SEAC4RS) field mission. Journal of Geophysical Research: Atmospheres, 121(9), pp.4967-5009, 2016.

Turnbull, J. C., Tans, P. P., Lehman, S. J., Baker, D., Conway, T. J., Chung, Y. S., Gregg, J., Miller, J. B., Southon, J. R., and Zhou, L. X.: Atmospheric observations of carbon monoxide and fossil fuel CO2 emissions from East Asia. Journal of Geophysical Research: Atmospheres, 116(D24), 2011.

United Nations, Department of Economic and Social Affairs, Population Division: The World's Cities in 2016 – Data Booklet (ST/ESA/ SER.A/392), 2016.

Van Leeuwen, T. T., and Van Der Werf, G. R.: Spatial and temporal variability in the ratio of trace gases emitted from biomass burning. Atmospheric Chemistry and Physics, 11(8), 3611-3629, 2011.

Vay, S.A., Woo, J.H., Anderson, B.E., Thornhill, K.L., Blake, D.R., Westberg, D.J., Kiley, C.M., Avery, M.A., Sachse, G.W., Streets, D.G. and Tsutsumi, Y.: Influence of regional-scale anthropogenic emissions on CO2 distributions over the western North Pacific. Journal of Geophysical Research: Atmospheres (1984–2012), 108(D20), 2003.

Vay, S.A., Choi, Y., Vadrevu, K.P., Blake, D.R., Tyler, S.C., Wisthaler, A., Hecobian, A., Kondo, Y., Diskin, G.S., Sachse, G.W. and Woo, J.H.: Patterns of CO2 and radiocarbon across high northern latitudes during International Polar Year 2008. Journal of Geophysical Research: Atmospheres, 116(D14), 2011.

Wachter, E. D., Barret, B., Flochmoën, E. L., Pavelin, E., Matricardi, M., Clerbaux, C., Hadji-Lazaro, J., George, M., Hurtmans, D., Coheur, P. F. and Nedelec, P.: Retrieval of MetOp-A/IASI CO profiles and validation with MOZAIC data. Atmospheric Measurement Techniques, 5(11), 2843-2857, 2012.

Wang, Y., Munger, J. W., Xu, S., McElroy, M. B., Hao, J., Nielsen, C. P., and Ma, H.: CO 2 and its correlation with CO at a rural site near Beijing: implications for combustion efficiency in China. Atmospheric Chemistry and Physics, 10(18), 8881-8897, 2010.

Ward, D. E., and Hardy, C. C.: Smoke emissions from wildland fires. Environment International, 17(2-3), 117-134, 1991.

Wunch, D., Wennberg, P. O., Toon, G. C., Connor, B. J., Fisher, B., Osterman, G. B., Frankenberg, C., Mandrake, L., O'Dell, C., Ahonen, P. and Biraud, S. C. A method for evaluating bias in global measurements of CO 2 total columns from space. Atmospheric Chemistry and Physics, 11(23), 12317-12337, 2011.

Warner, J.X., Wei, Z., Strow, L.L., Barnet, C.D., Sparling, L.C., Diskin, G. and Sachse, G.: Improved agreement of AIRS tropospheric carbon monoxide products with other EOS sensors using optimal estimation retrievals. Atmospheric Chemistry and Physics, 10(19), pp.9521-9533, 2010.

Wunch, D., Toon, G. C., Blavier, J. F. L., Washenfelder, R. A., Notholt, J., Connor, B. J., Griffith, D.W., Sherlock, V. and Wennberg, P. O.: The total carbon column observing network. Philosophical Transactions of the Royal Society of London A: Mathematical, Physical and Engineering Sciences, 369(1943), 2087-2112, 2011.

Yang, X. J.: China's rapid urbanization. Science, 342(6156), 310-310, 2013.

Yokota, T., Oguma, H., Morino, I., and Inoue, G.: A nadir looking SWIR FTS to monitor CO2 column density for Japanese GOSAT project, Proc. Twenty-fourth Int. Sympo. on Space Technol. And Sci. (Selected Papers), 887–889, 2004.

Yokota, T., Yoshida, Y., Eguchi, N., Ota, Y., Tanaka, T., Watanabe, H. and Maksyutov, S. Global concentrations of CO2 and CH4 retrieved from GOSAT: First preliminary results. Sola, 5, pp.160-163, 2009.

Atmos. Chem. Phys. Discuss., https://doi.org/10.5194/acp-2018-71
Manuscript under review for journal Atmos. Chem. Phys.
Discussion started: 26 January 2018

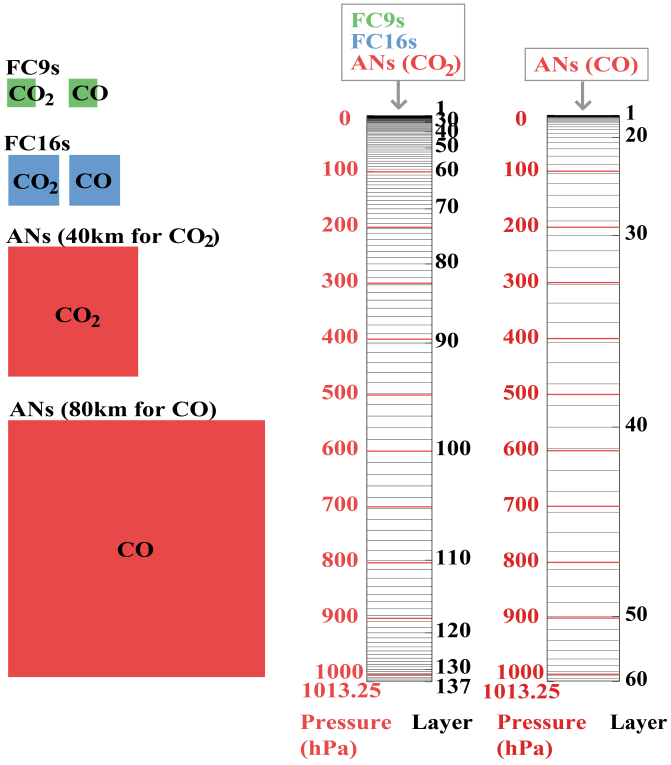

Figure 1. Model grid sizes of the CAMS and vertical structures of the model layers assuming the surface pressure being 1013.25hPa. FC9s, FC16s, and ANs for CO_2 (40 km) have 137 vertical layers. ANs for CO (80 km) have 60 vertical layers.

Atmos. Chem. Phys. Discuss., https://doi.org/10.5194/acp-2018-71
Manuscript under review for journal Atmos. Chem. Phys.
Discussion started: 26 January 2018

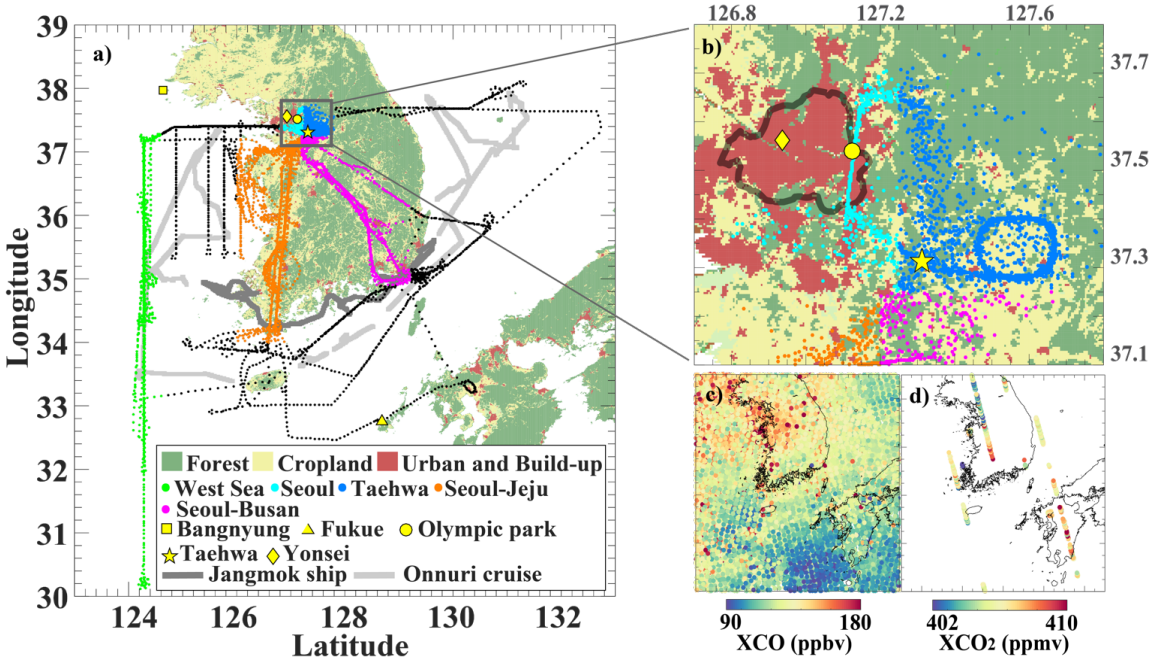

Figure 2. Domain of the study and KORUS-AQ measurements used in this study. Panel (a) shows land cover of the domain (Broxton et al., 2014), DC-8 aircraft tracks, ship tracks, and location of ground sites. The airborne measurements are classified into 5 groups (West Sea, Seoul, Taehwa, Seoul-Jeju jetway, and Seoul-Busan jetway), as marked in luminous green, luminous blue, mazarine blue, orange, and magenta. The ground sites are labelled with luminous yellow markers. Olympic park and Yonsei sites are located in urban regions (Seoul) while Baengnyeong and Fukue site are located in remote regions. Taehwa site is located in a forest nearby Seoul. Tracks of the two ships are marked in dark grey (Jangmok ship) and light grey (Onnuri ship). Also shown in (b) is the zoomed-in version of the grey box in panel (a). Panel (c) shows a composite MOPITT XCO retrievals during KORUS-AQ campaign while panel (d) shows OCO-2 XCO_2 retrievals in the same time period.

Atmos. Chem. Phys. Discuss., https://doi.org/10.5194/acp-2018-71
Manuscript under review for journal Atmos. Chem. Phys.
Discussion started: 26 January 2018

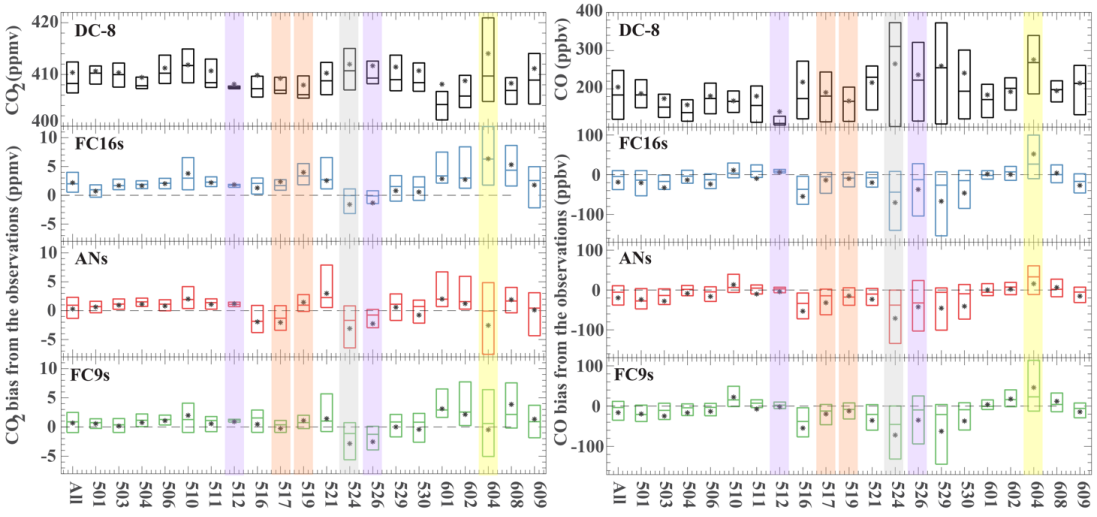

Figure 3. Boxplot for each individual flight. The flight date (MDD) for each boxplot is indicated in the bottom x-axis. Note that the dates here are in UTC time instead of Korea time. The left panel is for CO_2 and the right panel is for CO. The first row corresponds to the boxplot of the abundances measured by DC-8 aircraft. The second, third, and fourth rows correspond to the boxplot of the bias of FC16s, ANs, and FC9s relative to DC-8, respectively. The purple shade marks the flights with frontal passage, and orange shade marks the flights that may possibly be affected by biomass burning. The grey shade marks the flight measuring China outflow while yellow shade marks the flight surveying point emission sources.

Atmos. Chem. Phys. Discuss., https://doi.org/10.5194/acp-2018-71
Manuscript under review for journal Atmos. Chem. Phys.
Discussion started: 26 January 2018

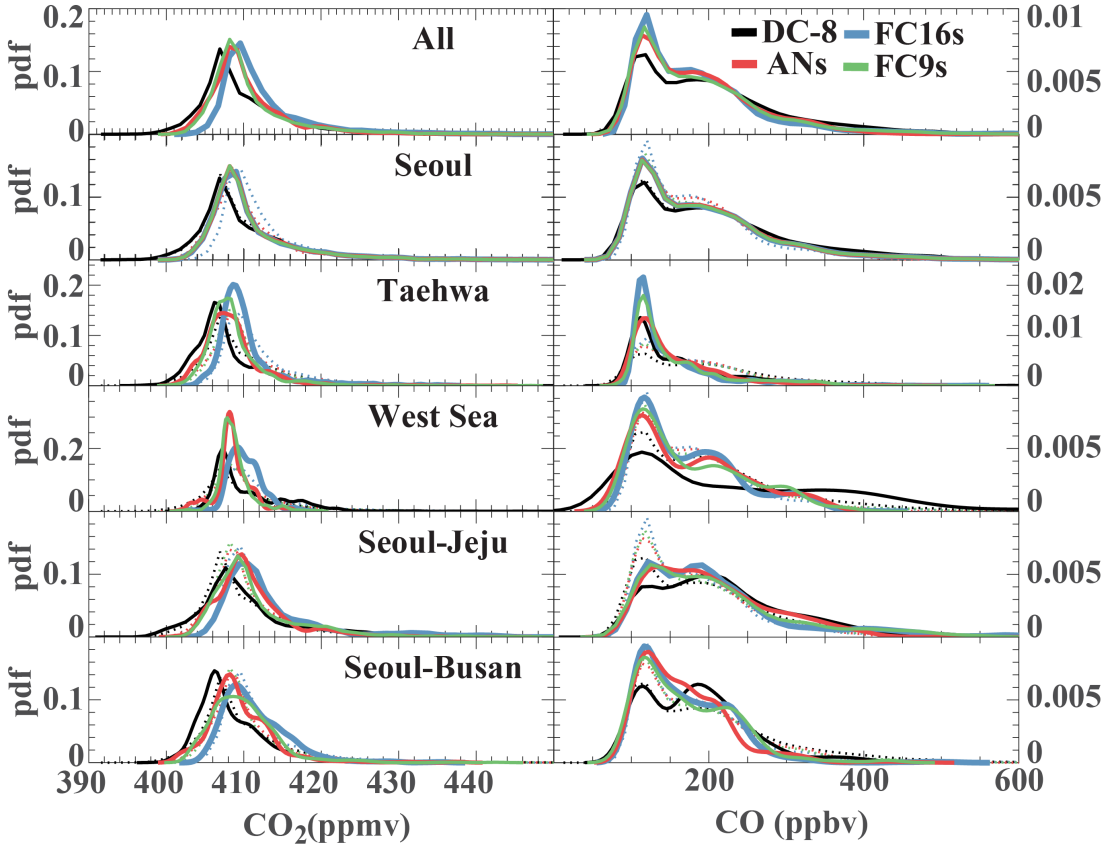

Figure 4. Probability density functions (pdfs) of CO_2 and CO for each flight group. Solid lines are pdfs for each group while the dashed lines are pdfs for all groups.

5

Atmos. Chem. Phys. Discuss., https://doi.org/10.5194/acp-2018-71
Manuscript under review for journal Atmos. Chem. Phys.
Discussion started: 26 January 2018

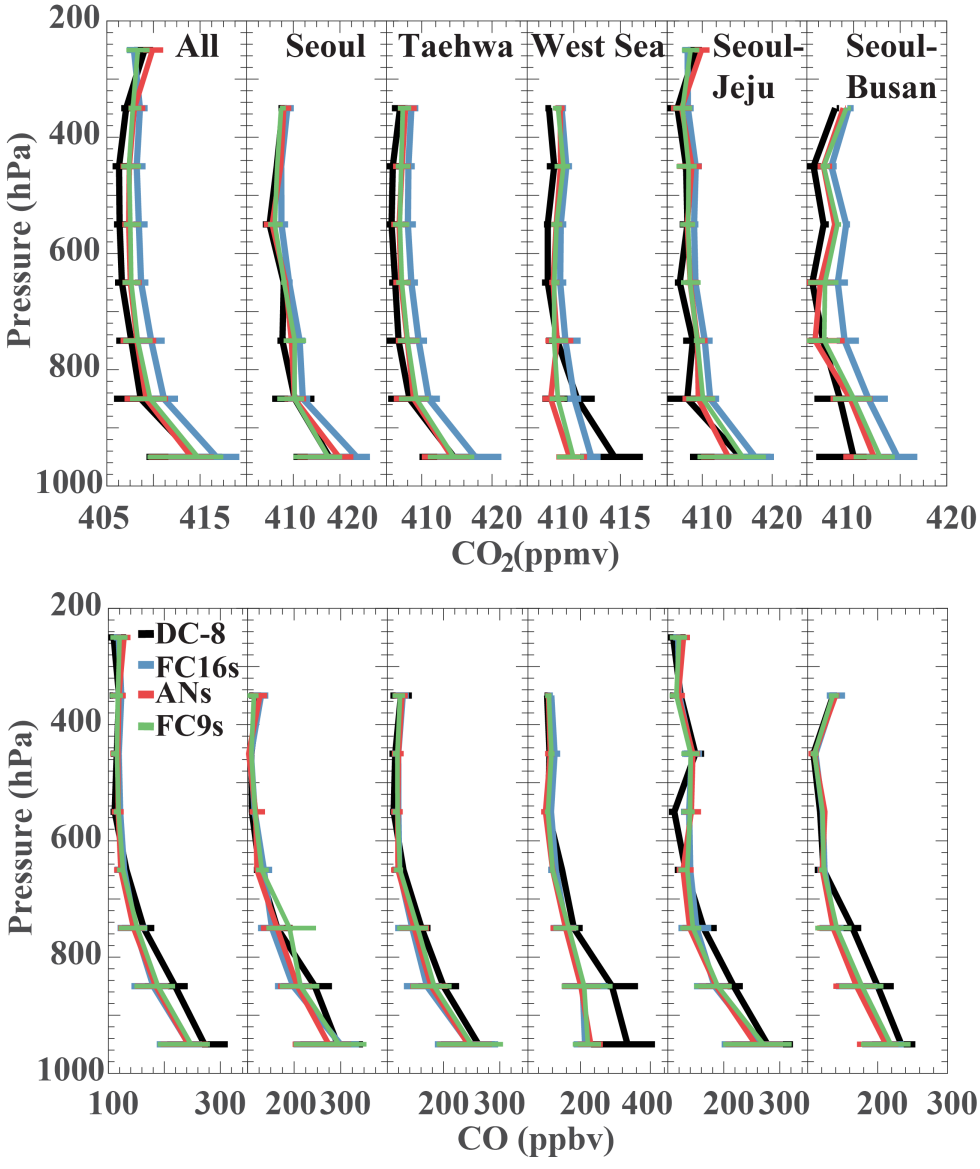

Figure 5. Averaged vertical profiles of CO_2 and CO mixing ratios from DC-8 and CAMS for each flight group. Horizontal bars correspond to the interquartile ranges (between 25th and 75th percentiles) of the layer bin.

Atmos. Chem. Phys. Discuss., https://doi.org/10.5194/acp-2018-71
Manuscript under review for journal Atmos. Chem. Phys.
Discussion started: 26 January 2018

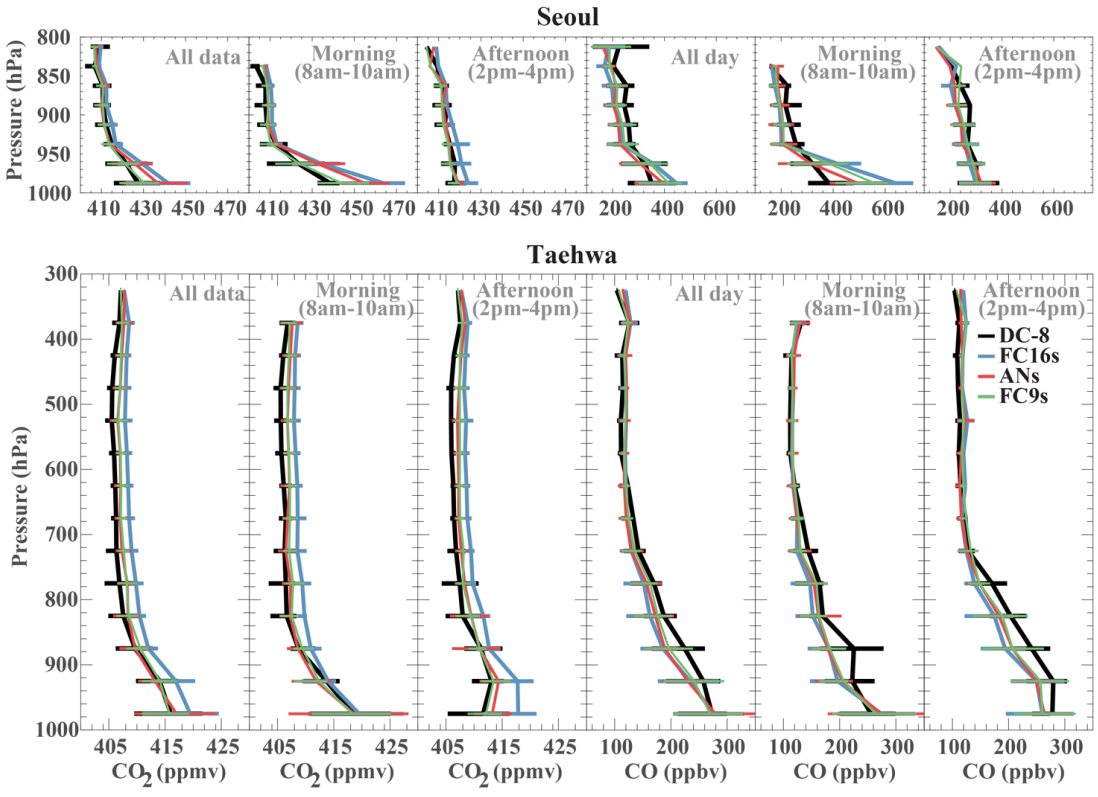

Figure 6. Temporal variation of averaged vertical profiles of CO_2 and CO mixing ratios from DC-8 and CAMS over Seoul and Taehwa flight groups. The first, second, and third columns are averaged CO_2 profiles for all day, morning (8-10am), and afternoon (2-4pm), respectively. Horizontal bars correspond to interquartile ranges (between 25th and 75th percentiles) of the profiles. The fourth, fifth, and sixth column are the same as the first three columns but for CO.

Atmos. Chem. Phys. Discuss., https://doi.org/10.5194/acp-2018-71
Manuscript under review for journal Atmos. Chem. Phys.
Discussion started: 26 January 2018

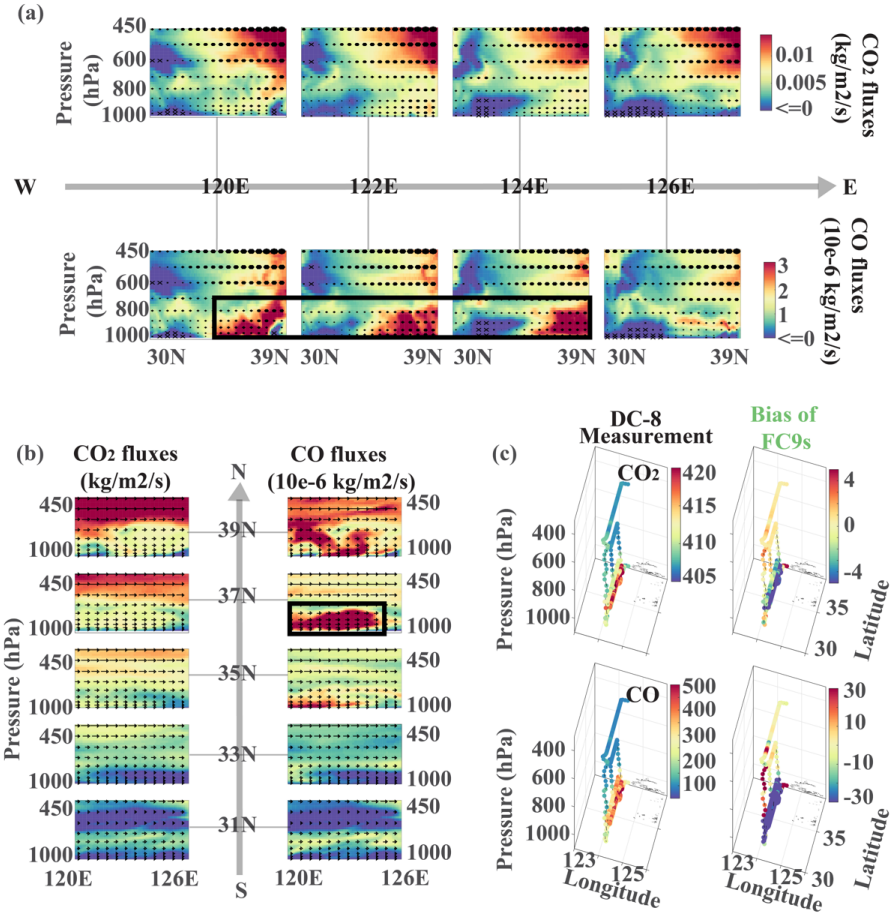

Figure 7. Case study for the flight on May 24th (UTC time). (a) Vertical distributions (hereafter denoted as 'sections') of fluxes (kg/m^2/s) at 9:00 am on May 25th (Korea time) in meridional direction. Dots represent meridional winds going from west to east (i.e., from China to Korea) and crosses represent meridional winds with the opposite direction. Sizes of the dots and crosses are proportional to the wind speed. 'Sections' on the top are for CO_2 fluxes and the bottom are for CO fluxes. (b) 'Sections' of fluxes (kg/m2/s) at 9:00 am on May 25th (Korea time) in zonal direction. Arrows represent meridional winds. 'Sections' in panel (b) share the same colorbar as panel (a). (c) DC-8 aircraft measurements (left column) and bias of CAMS along the flight track over West Sea (right column). The top row is for CO_2 and bottom row is for CO.

Atmos. Chem. Phys. Discuss., https://doi.org/10.5194/acp-2018-71
Manuscript under review for journal Atmos. Chem. Phys.
Discussion started: 26 January 2018

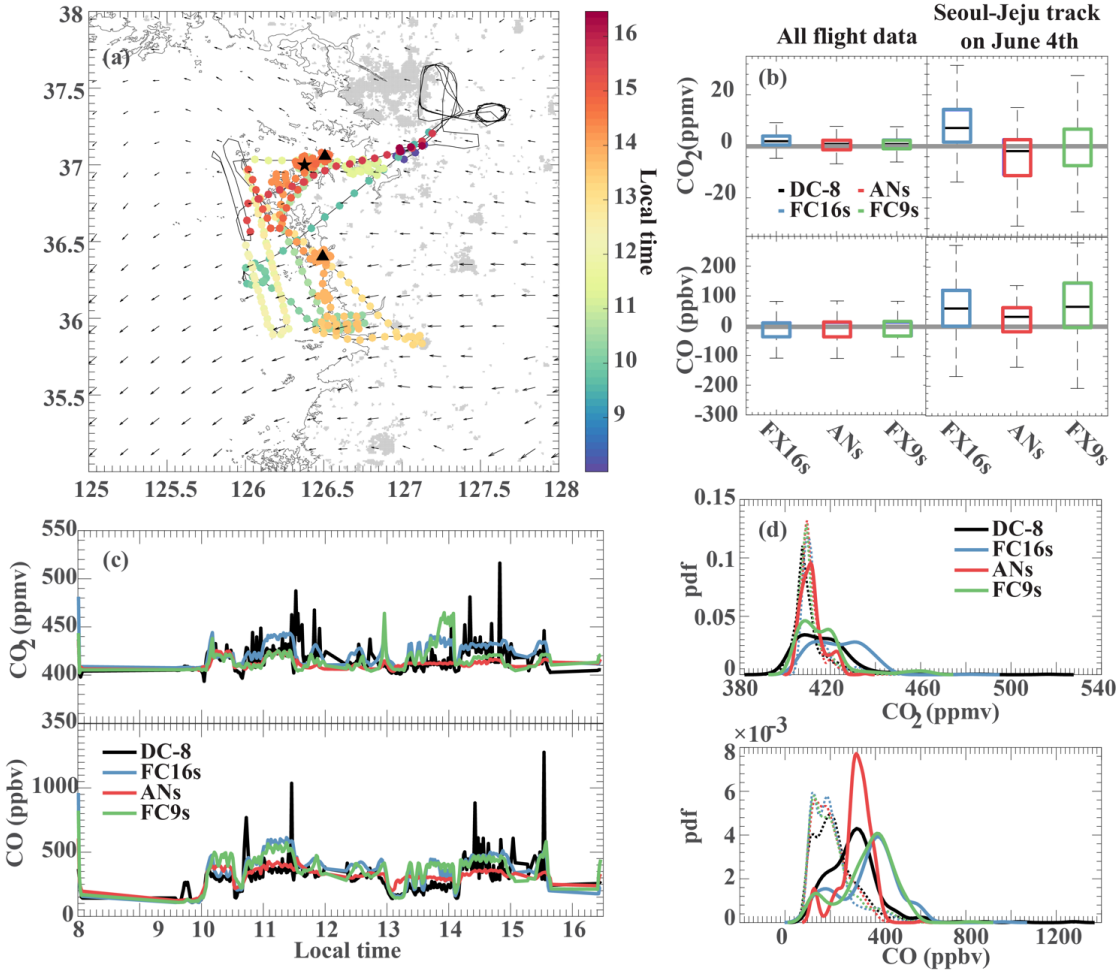

Figure 8. Case study for the flight on June 4th (UTC time). (a) Flight track of DC-8 aircraft in the Seoul-Jeju jetway group for this day. The Daesan chemical facility is marked as black pentagram and two power plants are marked as black triangles. Arrows correspond to 950 hPa wind field at 12:00pm local time. (b) Boxplot of CAMS bias from all the DC-8 aircraft measurements during the campaign (left), and from measurements on June 4th in the Seoul-Jeju jetway group (right). Top row is for CO_2 and bottom row is for CO. (c) Time series of DC-8 aircraft measurements and CAMS during the flight. (d) pdfs of CO and CO_2 for measurements on June 4th of the Seoul-Jeju jetway group (solid) and for all groups (dashed).

Atmos. Chem. Phys. Discuss., https://doi.org/10.5194/acp-2018-71
Manuscript under review for journal Atmos. Chem. Phys.
Discussion started: 26 January 2018

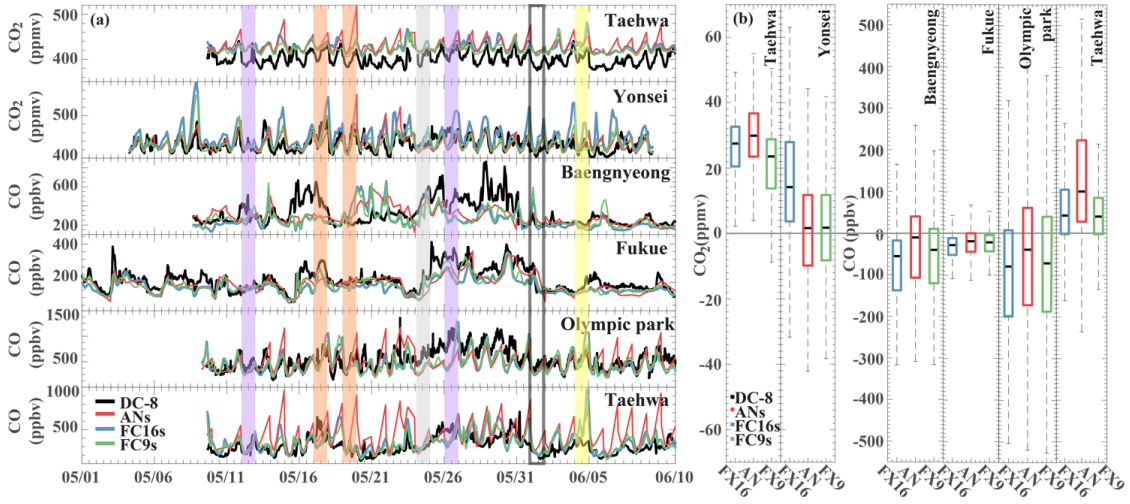

Figure 9. Comparisons of CAMS against ground site measurements. Values of CAMS are averages across layers with pressure higher than 95% of the surface pressure. (a) Time series of measured and CAMS CO_2 from the Taehwa and Yonsei sites, and CO from the Bangnyung, Fukue, Olympic park, and Taehwa sites. Shades denote same events as they do in Fig. 3. (b) Boxplot of CAMS bias for CO_2 at the Taehwa and Yonsei site measurements, and for CO at the Bangnyung, Fukue, Olympic park, and Taehwa sites.

Atmos. Chem. Phys. Discuss., https://doi.org/10.5194/acp-2018-71
Manuscript under review for journal Atmos. Chem. Phys.
Discussion started: 26 January 2018

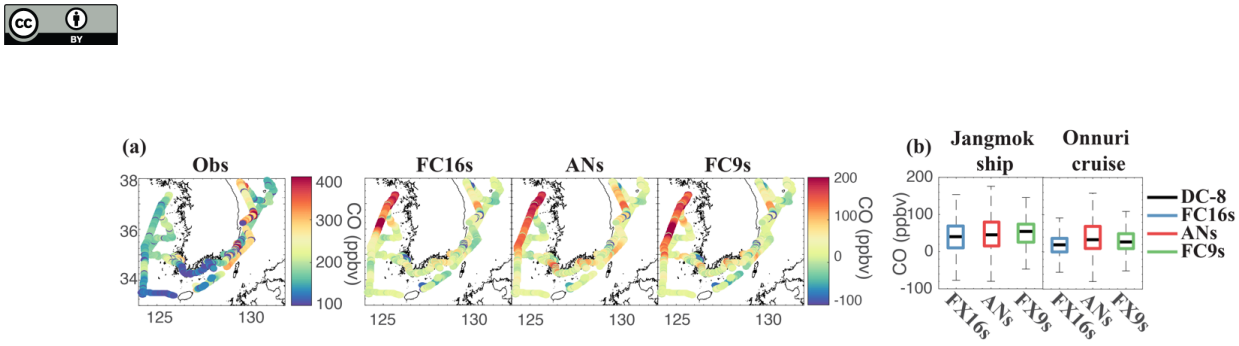

Figure 10. Comparisons of CAMS CO against ship measurements. Values of CAMS are averages across layers with pressure higher than 95% of the surface pressure. (a) Bias of CAMS CO against ship measurements along the ship track. (b) Boxplot of CAMS bias for CO compared with ship measurements.

Atmos. Chem. Phys. Discuss., https://doi.org/10.5194/acp-2018-71
Manuscript under review for journal Atmos. Chem. Phys.
Discussion started: 26 January 2018

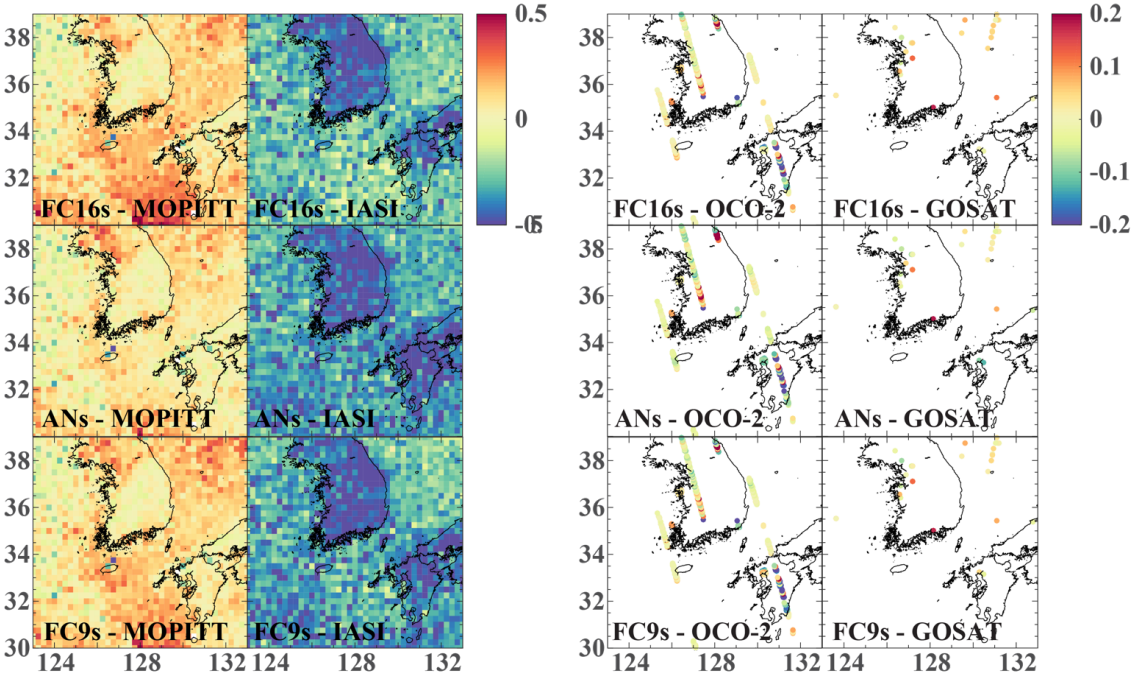

Figure 11. Spatial distributions of CAMS bias against satellite retrievals. For XCO, the unit is 10^{18} molecules/cm^2 while for XCO_2, the unit is 10^{21} molecules/cm^2.

Atmos. Chem. Phys. Discuss., https://doi.org/10.5194/acp-2018-71
Manuscript under review for journal Atmos. Chem. Phys.
Discussion started: 26 January 2018

Atmospheric Chemistry and Physics Discussions

Table1. Configuration of CAMS global atmospheric composition products valid during the period of the KORUS-AQ Field Campaign (May to June 2016). The tracers evaluated in this paper are highlighted in bold face. Time availability is in number of days with respect to real time (N/A is used when this is not applicable).

CAMS product	Atmospheric composition tracers	Horizontal resolution	Number vertical levels	Initial conditions: Meteorology	Initial conditions: Atmospheric composition	Time availability observations/analysis of atmospheric composition	Time availability of product
AN_CHEM	Reactive gases (**CO**,O3,NO_2,etc) and aerosols	80 km	L60	Own analysis	Own analysis	<1day	<1day
FC_CHEM	Reactive gases (**CO**,O3,NO_2,etc) and aerosols	80 km	L60	AN_CHEM	AN_CHEM	<1day	0 days (real time)
AN_GHG	**CO_2**, CH_4	40 km	L137	Own analysis	Own analysis	2-4 days	4 days
FC16s	**CO_2**, CH_4 and **linCO**	16 km	L137	ECMWF operational analysis	Previous 1-day forecast	N/A	1 day
FC9s	**CO_2**, CH_4, **linCO** and tagged tracers	9 km	L137	ECMWF operational analysis	AN_GHG 4-day fc for CO_2/CH_4 and AN_CHEM for linCO	4 day for AN_GHG; <1day for AN_CHEM	1 day

Atmos. Chem. Phys. Discuss., https://doi.org/10.5194/acp-2018-71
Manuscript under review for journal Atmos. Chem. Phys.
Discussion started: 26 January 2018

Atmospheric Chemistry and Physics Discussions

Table 2. Measurements during KORUS-AQ.

			CO_2	CO
Airborne measurements	NASA DC-8 aircraft	Instrument	LI-COR	DACOM
		Time Response	1 second	1 second
		Precision	< 0.1 ppmv	< 1% or 0.1 ppbv
		Accuracy	0.25 ppmv (Vay et al., 2003)	2% (Warner et al., 2010)
Ground site measurements	Baengnyeong (37.97N,124.63E)	Instrument	/	Teledyne Gas analyzer
		Data intervals	/	1 hour
	Fukue (32.75N,128.68E)	Instrument	/	48C
		Data intervals	/	1 hour
	Olympic Park (37.52N,127.12E)	Instrument	/	KENTEK CO analyzer
		Data intervals	/	5 minutes
	Taehwa (37.31N,127.31E)	Instrument	LI-COR LI-7500	Thermo 48i
		Data intervals	1 hour	1 hour
	Yonsei (37.56N, 126.94E)	Instrument	G2201-I CO_2/CH_4 carbon stable isotope analyzer	/
		Data intervals	30 minutes	/
Ship measurements	R/V Jangmok	Instrument	/	Thermo 48i-TLE
		Data intervals	/	1 minute
	R/V Onnuri	Instrument	/	Thermo Scientific, Inc., Model 48C
		Data intervals	/	1 minute
Satellite measurements	OCO-2		OCO-2	/
		Date product	Level 2 v7 Full Product XCO_2	/
		Resolution	2.25x1.29-km Global coverage ~16 days	/
		Revisit time	1:18 - 1:33 pm	/
		Uncertainty	1-2 ppm XCO_2 (Boesch et al., 2011 and references therein)	/
	GOSAT	Date product	Level 2 V02	/

		Resolution	10.5 x 10.5 km	/
			~12 days	
		Revisit time	~1:00 pm	/
		Uncertainty	2 ppm for retrieval errors of XCO_2	/
			Griffith et al. 2011; Crisp et al. 2012	
	MOPITT	Date product	/	TIR/NIR Level 2 v6 XCO
		Resolution	/	22 x 22 km
				~3-4 days
		Revisit time	/	10:30 am
		Uncertainty	/	0.09e18 molecules/cm^2 for total column retrieval; (Deeter et al., 2014)
	IASI	Date product	/	Level 2 FORLI XCO
		Resolution	/	12 km x 12 km
				twice a day
		Revisit time	/	
		Uncertainty	/	<13% for FORLI (Wachter et al., 2012)

Atmos. Chem. Phys. Discuss., https://doi.org/10.5194/acp-2018-71
Manuscript under review for journal Atmos. Chem. Phys.
Discussion started: 26 January 2018

Atmospheric Chemistry and Physics Discussions

Table 3. Statistics of CAMS performance evaluated against satellite observations.

		Seoul	Taehwa	West Sea	Seoul-Jeju	Seoul-Busan	All
$\Delta CO/\Delta CO_2$ (ppbv/ppmv)	DC-8 measurement	9.09±0.48	15.3±0.56	28.17±0.75	10.37±0.31	15.86±0.73	13.29±0.21
	FC16s	9.84±0.29	14.31±0.40	30.86±1.64	13.00±0.27	13.39±0.51	12.28±0.15
	ANs	8.21±0.45	13.71±0.48	30.60±1.73	14.98±0.45	12.68±0.47	12.60±0.2
	FC9s	11.56±0.62	16.06±0.57	32.44±1.77	11.68±0.35	13.87±0.54	12.52±0.2
Correlation of CO and CO_2	DC-8 measurement	0.78	0.68	0.89	0.62	0.60	0.66
	FC16s	0.94	0.83	0.42	0.83	0.74	0.82
	ANs	0.77	0.71	0.25	0.61	0.76	0.63
	FC9s	0.78	0.70	0.36	0.60	0.73	0.65
Correlation of $Bias_{CO}$ and $Bias_{CO_2}$	FC16s	0.90	0.61	0.80	0.46	0.55	0.61
	ANs	0.66	0.59	0.82	0.36	0.63	0.51
	FC9s	0.64	0.52	0.82	0.33	0.54	0.49

Atmos. Chem. Phys. Discuss., https://doi.org/10.5194/acp-2018-71
Manuscript under review for journal Atmos. Chem. Phys.
Discussion started: 26 January 2018

Atmospheric Chemistry and Physics Discussions

Table 4. Statistics of CAMS performance compared against satellite observations.

		CO		CO_2	
		MOPITT	IASI	OCO-2	GOSAT
total observations during campaign		13612	25509	4591	42
bias (molecules/cm^2)	FC16s	-1.13E+17	8.28E+16	9.30E+18	-2.64E+19
	ANs	-6.42E+16	1.36E+17	4.48E+19	1.05E+19
	FC9s	-1.01E+17	7.52E+16	-1.31E+19	-1.28E+19
RMSE (molecules/cm^2)	FC16s	2.47E+17	4.19E+17	7.11E+19	5.67E+19
	ANs	2.31E+17	4.12E+17	8.48E+19	6.42E+19
	FC9s	2.56E+17	4.19E+17	8.29E+19	5.49E+19
correlation	FC16s	0.65	0.44	0.88	0.78
	ANs	0.66	0.52	0.85	0.63
	FC9s	0.61	0.45	0.85	0.75